Two classes of His-Me finger superfamily nuclease effectors exerting synergy for *Agrobacterium* T6SS-mediated interbacterial competition

Mary Nia M. Santos[a1], Katherine L. Pintor[a2], Pei-Yu Hsieh[b3], Yee-Wai Cheung[a], Li-Kang Sung[a], Yu-Ling Shih[b] and Erh-Min Lai[a*]

[a] Institute of Plant and Microbial Biology, Academia Sinica, Taipei 115201 Taiwan
[b] Institute of Biological Chemistry, Academia Sinica, Taipei 115201 Taiwan

Running title: His-Me finger T6SS nuclease toxins

*Corresponding author
Erh-Min Lai: emlai@gate.sinica.edu.tw
Institute of Plant and Microbial Biology, Academia Sinica
128 Sec. 2, Academia Road, Nankang, Taipei, Taiwan 115201

Current address:
[1]Aquaculture Research and Development Division, Department of Agriculture - National Fisheries Research and Development Institute (DA-NFRDI), Manila, Philippines
[2]Department of Ecophysiology, Max Planck Institute for Terrestrial Microbiology, Karl-von-Frisch-Str. 10, 35043 Marburg, Germany
[3]Department of Pharmacology, University of Cambridge, United Kingdom

ORCID
MNMS https://orcid.org/0000-0001-6544-0339
KLP https://orcid.org/0000-0001-9137-4726
PYH https://orcid.org/0000-0002-7263-1691
YWC https://orcid.org/0000-0002-1421-4419
LKS https://orcid.org/0000-0002-7078-8003
YLS https://orcid.org/0000-0002-8232-2569
EML https://orcid.org/0000-0003-3630-8683

ABSTRACT

Type VI secretion system (T6SS) assembles into a contractile nanomachine to inject effectors across bacterial membranes for secretion. *Agrobacterium tumefaciens* species complex is a group of soil inhabitants and phytopathogens that deploys T6SS as an antibacterial weapon against bacterial competitors at both inter-species and intra-species levels. *A. tumefaciens* strain 1D1609 genome encodes four effector genes, in which all four are specialized effector harboring a conserved N-terminal PAAR-like DUF4150 domain but distinct C-terminal effector domains. Previous study reported that V2a is a His-Me finger nuclease toxin contributing to DNase-mediated antibacterial activity. However, it remains unknown about the functions and roles of other three effectors. In this study, we identified V2c is another His-Me finger nuclease encoded by 1D1609 genome but with distinct SHH motif differed from AHH motif of V2a. We demonstrated that the ectopic expression of V2c caused growth inhibition, plasmid DNA degradation, and cell elongation in *Escherichia coli*. The cognate immunity protein, V3c, neutralizes the DNase activity and rescues phenotypes of the growth inhibition and cell elongation. Ectopic expression of V2c DNase-inactive variants retain the cell elongation phenotype while V2a induced cell elongation in a DNase-mediated manner. We also showed that the amino acids of conserved SHH and HNH motifs are responsible for the V2c DNase activity *in vivo* and *in vitro*. Notably, V2c also mediated the DNA degradation and cell elongation of target cell in the context of interbacterial competition. Importantly, V2a and V2c function synergistically to exert stronger antibacterial activity against the soft rot phytopathogen, *Dickeya dadantii*.

INTRODUCTION

The type VI secretion system (T6SS) is a nanomachine used by many gram-negative bacteria for antagonism or pathogenesis by injecting toxins into target bacterial or eukaryotic cells. T6SS is composed of a membrane complex in connection to a baseplate, which is the docking site for polymerization of a tube surrounded by a contractile sheath (1). The tube is stacked of Hcp protein hexamer tipped with the trimeric VgrG puncturing device and a PAAR repeat-containing protein which sharpens the tip (2). When the sheath contracts, the tube is propelled towards the target cell to deliver effectors. After firing, the sheath disassemble and the subunits of the sheath are recycled to build another machine (3).

68

69 In terms of delivery, the T6SS effectors can be classified as cargo or specialized
70 effectors. The cargo effectors interact non-covalently with Hcp, VgrG or PAAR while
71 in specialized effectors, the effector domain is covalently fused to Hcp, VgrG or PAAR
72 (4). Functionally, most of the identified effectors mediate antibacterial activities
73 including nuclease, peptidoglycan hydrolase, lipase, phospholipase, NAD(P)+-
74 glycohydrolase and ADP ribosyltransferase by targeting conserved cellular structures
75 such as nucleic acids, peptidoglycan, and inner membrane as well as specific
76 metabolites or proteins (5).

77

78 *Agrobacterium tumefaciens* is a Gram-negative alphaproteobacteria belonging to the
79 Rhizobiaceae family. It is an economically important pathogen that causes crown gall
80 disease and a gene delivery tool with capability of transforming plant cells and fungi
81 (6). T6SS main gene cluster is highly conserved in the genome of *A. tumefaciens*
82 genomospecies complex (7, 8). Besides the main cluster consisting of two divergent
83 operons, *imp* (imp<u></u>aired in nitrogen fixation) encoding core structural and regulatory
84 components and *hcp* operon for effectors and effector delivery components (e.g. *hcp,*
85 *vgrG, paar*), most *A. tumefaciens* strains also encode one to multiple *vgrG* operons
86 encoding effector-immunity (EI) gene pairs. *A. tumefaciens* strain 1D1609 encodes
87 largest number of *vgrG* (*vgrGa, vgrGb, vgrGc, vgrGd*) in *A. tumefaciens*
88 genomospecies complex with each module associated with an EI pair (9). Previous
89 study by deletion of single or multiple *vgrG*-associated effector-immunity (EI) pairs
90 suggested that *vgrGa*-associated effector V2a appears to be the major antibacterial
91 toxin but other effectors also contribute to full antibacterial activity for 1D1609 (9). V2a
92 is a PAAR (DUF4150)-linked specialized DNase effector harboring C-terminal Tox-
93 AHH domain. It is a member of the HNH/ENDO VII nuclease superfamily, which also
94 named as His-Me finger endonuclease superfamily (9, 12, 13). This study also
95 indicated there are three more putative EI pair encoded in the other three orphan *vgrG*
96 modules. However, the biochemical and biological functions of other three EI pairs
97 remain uncharacterized.

98

99 In this study, we discovered that *vgrGc*-associated effector V2c is another DNase toxin
100 and explored the rationale of having two T6SS DNase toxins in *A. tumefaciens* strain
101 1D1609. We show that V2c harbors a DNase toxin domain with a conserved SHH

motif representing a newly characterized T6SS bacterial toxin. SHH is one of the five new clades identified in the His-Me finger nuclease superfamily (10). His-Me finger nucleases are characterized by their strictly conserved histidine (His) (1st H in the HNH motif) and a metal ion (Me) bound to conserved His (last H in the HNH motif) being essential for nucleic acid hydrolysis (11). Here, we show that the expression of V2c caused growth inhibition, plasmid DNA degradation and cell elongation, which the phenotypes are neutralized by co-expression of the cognate immunity protein, V3c. We also show that the SHH motif is responsible for the nuclease activity of V2c. Importantly, V2a AHH nuclease and V2c SHH nuclease function synergistically to exert stronger antibacterial activity against the soft rot phytopathogen, *Dickeya dadantii*. V2c orthologs are also conserved in Rhizobiaceae family, suggesting the importance of His-Me finger T6SS nuclease in this family for interbacterial competition.

RESULTS

V2c is a DNase belonging to the Tox-SHH clade of His-Me finger superfamily

Of the four identified effector-immunity (EI) pairs encoded on T6SS main and auxiliary clusters in *A. tumefaciens* 1D1609, *v2c* (At1D1609_43220) resides in the auxiliary cluster, upstream of its putative cognate immunity protein, *v3c* (At1D1609_43230) (9). V2c is a PAAR (DUF4150)-linked specialized effector (**Figure 1A**) that similar to V2a, the homolog encoded on the T6SS main cluster. Despite both V2a and V2c harboring N-terminal PAAR domain (**Figure S4**), V2c does not show any sequence similarity to V2a as well as other known T6SS effectors by BLAST and CDD searches. Multiple sequence alignment of V2c and V2c orthologs revealed V2c containing conserved SHH and HNH motifs at its C-terminal region (**Figure 1B**), in which these V2c orthologs all harbor C-terminal Tox-SHH domain but their N-terminal region can be fused to other known T6SS domains such as Found in type sIX effector (FIX) and FIX RhsA AHH HNH-like (14, **Figure 1C).** Using the protein homology detection program HHpred (15), we found that the C-terminal region of V2c encodes two parallel β-strands connected by α-helix, which is signature structure in His-Me finger nuclease (12). Consistent with the result of secondary structure prediction, structure prediction using AlphaFold (**Figure 1D**) shows this domain consists of two antiparallel β-strands connected with an Ω loop with a His (H384) at the C-terminus of the first β-strand and followed by an α-helix, featuring a HNH motif of His-Me finger endonuclease (10, 11).

134 These suggest V2c belonging to the Tox-SHH (Pfam PH15652) clade of His-Me finger
135 superfamily.
136
137 To demonstrate the antibacterial and DNase activities of V2c, we expressed *v2c* using
138 an arabinose inducible promoter to determine if V2c is a bacterial toxin functioning as
139 a nuclease. Growth inhibition measured by optical density was observed when *v2c* is
140 expressed by arabinose induction in *Escherichia coli* and this can be neutralized by
141 co-expression of its putative cognate immunity *v3c* as compared to the vector control
142 (**Figure 2A**). Also, colony forming unit (CFU) count shows the reduced CFU of *v2c*-
143 expressed cells and higher CFU could be recovered with co-expression of *v3c* (**Figure**
144 **2B**). In addition, plasmid degradation assay showed that the expression of *v2c* upon
145 arabinose induction resulted in degradation of plasmid DNA in *E. coli* and this is
146 abolished when *v3c* is co-expressed (**Figure 2C**). The data indicated that V2c exhibits
147 DNase activity *in vivo*.
148
149 We further investigated whether the SHH and HNH motif are involved in DNase activity.
150 His-Me finger superfamily has a strictly conserved His residue and catalytic metal ion
151 which are both essential for nucleic acid hydrolysis. Based on this premise, we define
152 a region that contains His residues as the putative catalytic site region as a His-Me
153 finger domain core region (CR), corresponding to the region spanning amino acid
154 residues 380-409. Based on the alignment, H384 is the catalytic His and H408 is for
155 metal ion binding while H383 may function as second residue for metal ion
156 coordination. To verify their roles in the His-Me finger domain, a series of deletion as
157 well as single and double amino acid substitution variants were generated. Strikingly,
158 no growth inhibition and plasmid degradation were observed in any of the mutants
159 expressing the CR deletion ($V2c^{CR}$), single ($V2c^{H383A}$, $V2c^{H384A}$ and $V2c^{H408A}$) and
160 double ($V2c^{HAHA,}$ substitution in both H383 and H384) variants (**Figure 2A, C, D**).
161 Higher CFU was also recovered from *E. coli* culture expressing these mutants alone
162 or with V3c (**Figure 2B**). To further confirm the DNase activity of V2c*,* each of V2c and
163 its variants is fused with 6x-His and purified for *in vitro* DNase activity assay. The
164 results showed that purified V2c fraction is able to degrade DNA, but not the eluate
165 from *E. coli* expressing the vector (pET28a) (**Figure 2D**). Consistent with the *in vivo*
166 plasmid degradation assay, no activity could be detected from $V2c^{H384A}$*,* $V2c^{H408A}$, or
167 $V2c^{HAHA}$ variants. However, purified $V2c^{H383A}$ fraction exhibited DNase activity by

168 degrading the plasmid DNA substrate. Western blot analysis of the reaction samples
169 shows V2c and its variants used for the assay were at similar protein levels. Taken the
170 results of *in vivo* and *in vitro* DNA degradation assays, the conserved H384 and H408
171 in the HNH motif are crucial for V2c DNase activity whereas H383 in SHH motif
172 appears to be less critical for *in vitro* but may be required for *in vivo* nuclease activity.

173 **Ectopic expression of V2c caused DNA degradation and cell elongation**

174 We next examined the cell morphology and DNA integrity of *E. coli* cells expressing
175 V2c and the two variants ($V2c^{CR}$ and $V2c^{H408A}$) that are defective in DNase activity and
176 toxicity. Cell morphology was observed by phase contrast while bacterial cell
177 membrane and DNA were stained by FM4-64 and Hoechst, respectively under
178 fluorescence microscope. Hoechst signals are significantly reduced when V2c is
179 expressed by arabinose induction in *E. coli* and this can be rescued by co-expression
180 of its cognate immunity V3c shown in the images and quantification (**Figure 3A, B**).
181 Hoechst signals are diminished only in *E. coli* cells producing *v2c* but not $v2c^{H383A}$
182 $v2c^{H384A}$, $v2c^{CR}$ and vector control, suggesting that the cellular DNA degradation is
183 caused by V2c DNase activity, which can be neutralized by its immunity protein V3c.
184
185 In addition, we also observed cell elongation in *E. coli* expressing *v2c* (**Figure 3A, C**).
186 Notably, co-expression of V3c rescues the cell elongation phenotype. However, *E. coli*
187 expressing $v2c^{CR}$ and $v2c^{H408A}$ does not abolish the elongated cell phenotype (**Figure**
188 **3A, C**).

189 **Ectopic expression of V2a also caused cell elongation phenotype**

190 Previous study showed that V2a is a Tox-AHH nuclease that serves as the major
191 antibacterial weapon in 1D1609 (9). H385 and H386 are two of the predicted His
192 residues in AHH motif of V2a, corresponding to H383 and H384 in SHH motif of V2c.
193 The structure predicted by AlphaFold indicates V2a also featuring a His-Me finger, in
194 which two α-helices with histidine residues (H430, H456) followed the β-strands
195 (**Figure 4A**). And, our previous findings demonstrated that expression of V2a but not
196 $V2a^{H385A}$ caused growth inhibition and plasmid degradation in *E. coli* (9). To gather
197 further insight of V2a AHH motif in the His-Me finger domain, we evaluated the
198 growth and morphology of arabinose induced V2a mutants. Results showed that
199 expression of V2a caused reduction in Hoechst-stained DNA signals and resulted in

200 cell elongation (**Figure 4B, C, D**). The expression of V2a^{H385A} has similar levels of
201 Hoechst-stained DNA signals and cell length as compared to the vector control.
202 These results suggest that the cell elongation phenotype observed were caused by
203 V2a DNase activity, whereas V2c shows DNase activity-independent cell elongation.
204 We also determined the toxicity of another putative effector V4b of 1D1609, a PAAR
205 (DUF4150)-linked specialized effector but harboring a Rhs domain with structural
206 similarity to the insecticidal toxin (9) (**Figure S1A**). Expression of *v4b* caused growth
207 inhibition in *E. coli,* in which the growth inhibition can be rescued by co-expression of
208 its putative cognate immunity *v5b* to a level similar to vectors control (**Figure S1B**).
209 However, no DNA degradation and cell elongation could be observed (**Figure S1C,**
210 **D, E, F**). These results suggest that cell elongation phenotype may be specific to
211 toxicity of nuclease effectors and V4b may also function as a bacterial toxin.

212 **V2c and V2a nucleases function synergistically for antibacterial activity against**
213 **the soft rot phytopathogen, *Dickeya dadantii***

214 To correlate the DNA degradation and cell elongation phenotypes observed by ectopic
215 expression in *E. coli* in more biologically relevant context, we further performed
216 interbacterial competition assay using the phytopathogen, *Dickeya dadantii* 3937 as
217 the prey cells. Expression of TssB with a C-terminal fusion to green fluorescence
218 protein (TssB-GFP) has been shown to assemble into a functional TssBC sheath in *A.*
219 *tumefaciens* strain C58 (16). Here, we expressed 1D1609 TssB with a C-terminal
220 fusion to super-folder GFP (TssB-sfGFP) endogenously in both 1D1609 wild type
221 (WT::TssB-sfGFP) and a non-functional T6SS mutant lacking all four *vgrG* genes
222 (Δ*4*::TssB-sfGFP) (9). While a few GFP foci were also detected in Δ*4*::TssB-sfGFP,
223 the TssBC sheath structures and dynamics could only be observed in WT::TssB-
224 sfGFP cells (**Figure S2A**, **Supplementary video 1**), confirming TssBC sheath is not
225 formed in the mutant lacking all four *vgrG* genes. This is consistent with the lack of
226 Hcp secretion in Δ*4*::TssB-sfGFP although TssB-sfGFP fusion proteins are at similar
227 abundant in all strains (**Figure S2B**). Accordingly, some of *D. dadantii* prey cells (either
228 WT or Δ*imp,* a non-functional T6SS mutant) became elongated and were lysed after
229 competition with WT::TssB-sfGFP but not Δ*4*::TssB-sfGFP (**Figure 5A**).
230

231 Next, we constructed mutants lacking one or several EI pairs and used them to assess
232 the activity against *D. dadantii* Δ*imp* expressing GFP (*D. dadantii* Δ*imp*-GFP(S65T))

233 by microscopy and quantified the number of viable cells (log_{10} CFU/mL) after co-
234 culture with *D. dadantii* Δ*imp*. The use of *D. dadantii* 3937 Δ*imp* mutant is to avoid
235 potential counterattack by *D. dadantii* T6SS (16). We observed very few cells
236 expressing GFP when competing with WT or Δ*3EIbcd* expressing V2a effector only.
237 The lysed and elongated *D. dadantii* cells were only detected when co-cultured with
238 1D1609 with either strains expressing V2a only (Δ*3EIbcd*), V2c only (Δ*3EIabc*), or both
239 Δ*3EIbd* (**Figure 5B**). No lysed and elongated cells were observed in Δ*4EI* and *D.*
240 *dadantii* only.
241
242 By counting CFU of prey cells after Interbacterial competition, the results also show
243 that V2a only (Δ*3EIbcd*) exhibited similar antibacterial activity as the WT against *D.*
244 *dadantii* (**Figure 5C**). In addition, 1D1609 expressing V2c only (Δ*3EIabd*) showed
245 weak but detectable antibacterial activity as compared to Δ*4EI,* indicating V2c itself is
246 able to detoxify *D. dadantii* but with weaker activity than V2a. Strikingly, 1D1609
247 expressing V2a and V2c only (Δ*2EIbd*) could result in stronger killing effects than WT.
248 We further quantified the cell length under the fluorescence microscope after
249 competition assay and results showed that *D. dadantii* cells were elongated after 18
250 hours of co-culture with either *v2a* and *v2c* effectors, or combination of both, as
251 compared to those *D. dadantii* cells alone or co-incubated with Δ*4EI* (**Figure 5D**).
252 Taken together, these results suggest that 1D1609 uses the two V2a and V2c DNase
253 effectors with synergistic antibacterial activity against *D. dadantii* resulting to elongated
254 and lysed cells.

255 **DISCUSSION**

256 Nucleases are considered as one of the most potent categories of T6SS effectors
257 because they poison the targets from the most essential in the origin of life, nucleic
258 acid. Although His-Me finger nucleases are a large and diverse superfamily of
259 nucleases, however, only a limited number of T6SS effectors have been identified as
260 His-Me finger nuclease. In the present study, we characterized a T6SS effector in *A.*
261 *tumefaciens* strain 1D1609, V2c, by its DNase activity. Results shows V2c caused
262 DNA degradation both *in vivo* and *in vitro* (**Figure 2C, 2D**) that confirmed V2c is a
263 DNase. Moreover, our previous findings (9) suggest V2a and V2c that consisting of
264 Tox-AHH and Tox-SHH motifs respectively, belong to the His-Me finger superfamily.

265 The predicted structures (**Figure 1D, 4A**) show that both V2a and V2c contain the
266 signature structure of His-Me finger domain harboring the catalytic His located at the
267 C-terminus of their β1 strands (H384 for V2c and H386), which is predicted to be the
268 general base for hydrolysis of phosphodiester bonds, followed by α-helixes. With our
269 previous findings on V2a, these suggest both V2a and V2c are His-Me finger
270 nucleases.
271
272 Given that His-Me finger nucleases are one-metal-ion-dependent nucleases, primarily
273 dependent on Mg^{2+} or in some cases dependent on Zn^{2+}. H408 of V2c and H430 of
274 V2a are determined as the His residue for direct binding to metal ion whereas another
275 acidic or polar amino acid may also coordinate the metal ion, located before the
276 invariant His (first H in SHH or AHH motif), which could either be Asn/Asp/Glu or His
277 which preferentially bind to Mg^{2+} or Zn^{2+}, respectively (9). The latter is the case for
278 both V2a (AHH motif) and V2c (SHH motif). The two His (H383, H384) residues of V2c
279 SHH motif are both required for exerting DNase activity *in vivo,* consistent with the
280 requirement of H385 and H386 of V2a AHH motif for DNase activity (8). Different from
281 the loss of DNase activity *in vivo*, $V2c^{H383A}$ variant retains the DNase activity by an *in*
282 *vitro* nuclease activity assay (**Figure 2C, 2D**). This indicates the requirement of H383
283 in coordinating metal ion binding for DNase activity may be subject to environmental
284 factors. His-Me fingers approach DNA from the minor groove and clamp the phosphate
285 backbone via the α-helix and β1 strand. Apart from having similar DNA-binding modes,
286 His-Me finger nucleases also share a conserved catalytic mechanism for hydrolyzing
287 nucleic acids. They all cleave P-O3' bonds to generate cleaved products containing
288 5'-phosphate and 3'-OH ends (22). If both V2a and V2c have the same mechanism to
289 bind and hydrolyze DNA, then the other domains outside the His-Me finger fold may
290 explain the difference in the phenotype.
291
292 His-Me finger encodes a small structural motif, so it is usually associated with other
293 domain architectures that could play additional functions. In addition, its three-element
294 structural motif is unable to provide enough of a hydrophobic core for stability (10).
295 Thus, many proteins containing the His-Me finger employ a variety of additional
296 structural elements or domains for stabilization and/or specificity. As V2c and its
297 orthologs commonly found in Rhizobiaceae are not included in the 77 sequences with
298 conserved core regions of His-Me finger superfamily reported by Jablonska et al (10),

299 suggesting they are SHH motif variants belonging to SHH clade of His-Me finger
300 nuclease. Our evidence also suggests that V2c may represent a new branch of Tox-
301 SHH toxin family (Pfam PF15652), which includes proteins with additional domain
302 architectures (**Figure 1**). This includes PAAR-domain containing protein, Found in
303 type sIX effector (FIX) superfamily, and FIX RhsA AHH-HNH-like. Most of these are
304 conserved regions found in many bacterial toxin proteins. Moreover, these additional
305 domain(s) may facilitate the secretion of nuclease and affect its toxicity to the
306 competing cell. While both V2c and V2a harbor the conserved N-terminal DUF4150
307 PAAR-like domain, they share low sequence similarity in the C-terminal region
308 including the AHH or SHH motifs containing His-Me finger domain that may contribute
309 to the difference on toxicity strength and the role of DNase on cell elongation (**Figure**
310 **S4**). The protein structures predicted by AlphaFold reveal the structural difference
311 between V2c and V2a (**Figure 1C, S1B**). Moreover, His-Me finger motif is nearly a
312 stand-alone domain and separate from the DNA sequence-specific binding domains
313 (22, 23). Collectively, we discovered *A. tumefaciens* strain 1D1609 is equipped with
314 two T6SS nuclease effectors, V2a and V2c, that belong to His-Me finger superfamily.
315 The findings expand the variety of T6SS His-Me finger nucleases on top of those have
316 been functionally characterized (9, 17, 18, 19).
317
318 Cell elongation caused by T6SS-mediated nuclease effector have been reported (17,
319 24). Besides nuclease effectors, cell division arrest is also caused by non-nuclease
320 effectors. For example, a T6SS ADP-ribosyltransferase effector called Tre1 in *Serratia*
321 *proteamaculans* was reported to inactivate bacterial cell division Tre1 by modifying
322 arginine on FtsZ to block polymerization (25). We also observed the elongation
323 phenotype in ectopic expression of *v2c* in *E. coli* and in *D. dadantii* during interbacterial
324 competition. The proposed biological role of bacterial filamentation is mainly related to
325 stress response to thrive for survival (26). One of the conditions that lead to
326 filamentation is DNA damage. When the DNA is damaged, the SOS response is
327 induced and cells may delay the cell cycle and inhibit cell division until DNA repair and
328 replication are complete. In this study, while both V2a and V2c cause DNA degradation,
329 the mechanism of induced cell elongation seems to be different. For V2a, the cell
330 elongation phenotype is unobservable in DNase inactive mutant by disrupting H385,
331 the metal ion coordinating residue (**Figure 4**). This contrasts with V2c, wherein the
332 DNase activity is independent of cell elongation phenotype. Cell elongation could still

333 be observed when different DNase defective V2c mutant proteins were expressed.
334 (**Figure 3, Figure S3A**). In addition, co-expressing of V3c can restore V2c-induced
335 cell elongation back to normal cell length, but not to all the catalytic variants (**Figure**
336 **3C, S3B**). The data suggest that another domain outside the SHH catalytic region in
337 V2c is responsible for the cell elongation phenotype. Different from the nuclease
338 activity-dependent filamentation observed previously (17, 24) and V2a, V2c-induced
339 cell elongation independent of nuclease activity may represent a new mechanism of
340 stress response that yet to be elucidated. Future work by domain dissection is needed
341 to identify the domain that causing cell elongation.
342
343 To date, a few T6SS effectors were reported to contain SHH motif, including Tke4 of
344 *Pseudomonas putida* (20) and Txe4 of fish pathogen *Pseudomonas plecoglossicida*
345 strain XSDHY-P that exerting DNase-mediated toxicity when expressed in *E. coli* (21).
346 However, it remains unclear whether SHH and HNH motifs of these T6SS His-Me
347 finger nucleases are directly involved in interbacterial competition. Here, we
348 demonstrate the DNase activities related to both SHH and HNH motifs are critical
349 during interbacterial competition against the soft rot phytopathogen *D. dadantii*. We
350 also discovered V2a and V2c exert synergistic antibacterial activity against *D. dadantii*.
351 The strain 1D1609 is unique in *A. tumefaciens* species complex with multiple VgrG
352 spikes carrying different antibacterial effectors (9). Several studies showed that some
353 T6SS toxins can only exert toxicity in specific bacterial species (27, 28). For 1D1609,
354 V2c-mediated antibacterial activity was observed when against *D. dadantii* was acted
355 as a prey, whereas it was not observed when *E. coli* was used as a prey (9). On the
356 other hand, V2a appears to be the major antibacterial weapon for interbacterial
357 competition against either *E. coli* or *D. dadantii*. From the observation of the synergism
358 of V2a and V2c against *D. dadantii,* harboring multiple T6SS effectors in 1D1609 is an
359 advantage for the strain to maintain a growth competitiveness in different niches and
360 environments.
361
362 In conclusion, in the present study we identified V2c is SHH motif bearing His-Me
363 finger nuclease, which its DNase activity can be neutralize by its cognate immunity
364 protein, V3c. We also found that V2c mediated the DNA degradation and cell
365 elongation of target cell independently. Importantly, V2a and V2c function

366 synergistically to exert stronger antibacterial activity against the soft rot phytopathogen,
367 *D. dadantii* 3937.

368 MATERIALS AND METHODS

369 Bacterial strains and growth conditions

370 Bacterial strains and plasmids are listed in Table S1. *Escherichia coli* strains were
371 grown in LB medium at 37°C, *A. tumefaciens* strains in 523 medium at 25°C and *D.*
372 *dadantii* 3937 in LB medium at 30°C. Antibiotics were added when necessary: for *E.*
373 *coli*, 30 µg/mL gentamicin and 250 µg/mL streptomycin; for *D. dadantii* 50 µg/mL
374 gentamicin.
375

376 Molecular cloning

377 Plasmid pJN105 was used for expression of toxin genes and pTrc200 plasmid was
378 used for expression of immunity gene. PCR was amplified with KAPA HiFi HotStart
379 DNA Polymerase (Roche) using genomic DNA of *A. tumefaciens* 1D1609. The C-
380 terminal fusion of *tssB* with superfolder GFP (sfGFP) was constructed in pJQ200ks to
381 replace the endogenous *tssB* in WT and Δ*4*Δ*tssB* background. The primers used in
382 the study are listed in Table S2. Site directed mutagenesis was done using either DpnI
383 or Gibson Assembly (New England BioLabs), ligated using T4 ligase (Takara) and
384 transformed into chemically competent *E. coli* DH10B. Plasmid DNA was isolated
385 using QIAprep miniprep kit (Qiagen). All constructs were confirmed by sequencing.
386 The in-frame deletion mutants in *A. tumefaciens* were generated using a suicide
387 plasmid via double crossing over by electroporation or by conjugation as described (9).

388 Bioinformatic analysis

389 The orthologs of V2c were analyzed using amino acid sequences after the DUF4150
390 domain via BLASTP search. Multiple sequence alignment was performed using
391 MUSCLE or Multiple Sequence Comparison by Log- Expectation (29). Full length
392 sequences of the V2c orthologs were analyzed to obtain domain architectures from
393 Pfam database (30). The E-value threshold was set at 10^{-5}. HHpred and Swiss
394 Model were used for homology-based protein structure prediction while the
395 availability of protein structure predicted by AlphaFold was from the UniProt
396 database. Secondary structure prediction was done using default settings in
397 PSIPRED 4.0 Protein Structure Prediction Server/ DMPfold 1.0 Fast Mode.

398 **Growth inhibition assay**

399 Growth inhibition assay was performed as described previously (31). In brief, overnight
400 cultures of *E. coli* DH10B strain with vectors were adjusted to OD_{600}. 1 mM isopropyl
401 β-D-1- thiogalactopyranoside (IPTG, Amresco) was used to induce the expression of
402 the putative immunity protein. L-Arabinose (Ara, Sigma-Aldrich) was added to 0.2%
403 final concentration, to induce expression of the toxin. Cell growth was recorded every
404 hour at OD_{600}. Empty vectors were used as controls. The number of colony forming
405 units (log_{10} CFU/mL) was quantified in each sample grown on agar plates.

406 **Plasmid DNA degradation analysis in *E. coli* cells**

407 *In vivo* plasmid DNA degradation analysis was performed as described previously (31).
408 In brief, overnight cultures of *E. coli* DH10B strain with empty vectors or expressing
409 the effectors and mutants were harvested and adjusted to OD_{600} ~0.3. L-Arabinose
410 (0.2%, final concentration) was added to induce toxin expression and cultured for 2 h.
411 Equal amounts of cells were used for plasmid DNA extraction and equal volume of
412 extracted DNA was resolved in agarose gel followed by ethidium bromide staining and
413 visualized using Gel Doc XR+ UV Gel Documentation Molecular Imager Universal
414 Hood II (Bio-Rad).

415 **Cloning, expression and purification of V2c and mutants**

416 The effector gene *v2c* was constructed in pET28a plasmid and immunity gene *v3c*
417 was constructed in pTrc200 plasmid. Site directed mutagenesis were done by using
418 overlap extension PCR. Plasmid for expressing effector protein, V2c WT or its variants,
419 and plasmid for expressing immunity protein, V3c, were transformed into *E. coli*
420 BL21(DE3) for IPTG-induced co-expression. Bacterial culture was incubated at 37 °C
421 until OD_{600} reached 0.5, then 0.1 mM IPTG was added followed by 5-h expression at
422 37 °C. Pellets were collected, sonicated, and expressed proteins were purified by
423 using Ni Sepharose 6 Fast Flow histidine-tagged protein purification resin (Cytiva).
424 Briefly, cells were lysed in extraction buffer (50 mM Tris-Cl, pH7.5, 0.1 M NaCl, 20 mM
425 imidazole) and proteins were eluted by using elution buffer with up to 250 mM
426 imidazole in 50 mM Tris-Cl, pH7.5, 0.1 M NaCl.

427 ***In vitro* DNase activity assay**

428 A 10 µL reaction containing 200 ng of pTrc200HA plasmid DNA and 1× CutSmart
429 Buffer (NEB) with partially purified V2c or its variants normalized by the major V2c
430 protein band was incubated at 37°C for 1 hour. The digestion of DNA was
431 determined by agarose gel electrophoresis and visualized by SYBR Safe DNA gel
432 stain (Invitrogen). The reaction samples of V2c or its variants were scaled up for
433 Western blotting analysis as described (31). Anti-V2c antibody was generated in
434 rabbits against two V2c peptides, PFYWDFPNSQVGRD and KRIAMLRGDPTRYD
435 (indicated in Figure S1).

436 **Western blot analysis**

437 Western blot analysis was performed as described (ref). In general, proteins were
438 resolved by SDS-PAGE and transferred onto a PVDF membrane by using a transfer
439 apparatus (Bio-Rad). The membrane was probed with primary antibody against V2c
440 (1:4000), Hcp (1:2500), TssB (1:4000) and GFP (1:1000), followed by incubation with
441 horseradish peroxidase-conjugated anti-rabbit secondary antibody (Chemichem)
442 (1:25000) and visualized with the ECL system (Perkin-Elmer Life Science, Boston,
443 USA).

444 **Fluorescence microscopy and image analysis**

445 *E. coli* DH10B carrying the effector-expressing plasmids were grown overnight at 37°C.
446 Overnight cultures were sub-cultured with OD_{600} ~0.01. After 1 h, L-arabinose (Ara)
447 was added (0.2% final concentration) to induce toxin expression. Cultures were
448 harvested after an hour and resuspended with 30 µL PBS with 0.5 % Tween 20 (PBST).
449 Three µL of cells was placed on 2% agarose pad and imaged. To check the DNA
450 degradation, the same protocol was followed and live cells were stained with 2 µg/mL
451 Hoechst (Life Technologies, USA) and 1 µg/mL FM4-64FX (Invitrogen) for 5 mins and
452 washed with PBS to remove the excess dye.
453
454 For co-culture of *D. dadantii* Δ*imp*-GFP(S65T) with various 1D1609 EI pair mutants,
455 strains were mixed at 1:10 ratio on AK agar. This is an optimized growth medium,
456 named as *Agrobacterium* Kill-triggering, *Agrobacterium* kill-triggering (AK) medium (3
457 g K_2HPO_4, 1 g NaH_2PO_4, 1 g NH_4Cl, 0.15 g KCl, 9.76 g MES in 900 mL ddH_20, pH 5.5)
458 (24) and solidified by 2% (w/v) agar. Cells from 16 h co-culture were concentrated to
459 OD ~10 and spotted on 2% agarose pad.

460

461 Imaging was performed using an inverted fluorescent microscope (IX81, Olympus
462 Japan) with objective lens UPLSAPO 100XO (Olympus, Tokyo, Japan), DAPI (49000;
463 Chroma), GFP (49002; Chroma) and Cy3 (49005; Chroma) filter set and CCD camera
464 (ORCA-R2; Hamamatsu, Japan). The images were acquired using Olympus cellSens
465 Dimension software.

466

467 All the image analysis was done using Fiji analyze particles tool (32). The micrograph
468 of FM4-64 fluorescence was used to segment surfaces (i.e. individual bacterial cell)
469 with background subtraction and thresholding. Feret's diameter was used. The cell
470 length (μm) was determined from cumulative counts of three random frames per
471 sample. For quantification of cell degradation, the Hoechst intensity was normalized
472 using the formula intensity/unit area of cells, where intensity is major x minor x 3.14
473 (π).

474 **Interbacterial competition assay**

475 Bacterial competitions were carried out as described before (7). Briefly, overnight
476 culture of *A. tumefaciens* and *D. dadantii* Δ*imp* were mixed at a 10:1 attacker to target
477 ratio and spotted on AK agar plates. The target strain harbor pRL662-GFP (S65T).
478 After 18 h incubation at 25°C, the co-cultured cells were collected, serially diluted and
479 plated on LB agar containing gentamicin to quantify surviving *D. dadantii* Δ*imp* by
480 counting CFU.

481 **Statistical analysis**

482 The statistical analyses were done using GraphPad Prism version 6.01 for Windows,
483 GraphPad Software, La Jolla California USA (www.graphpad.com). The number of
484 technical replicates and independent biological replicates, p values and statistical
485 tests performed are indicated in the figure legends. The mean of independent
486 replicates was compared using the following statistical tests: Student's t test, one-
487 way ANOVA followed by Tukey's multiple comparisons tests
488 (http://astatsa.com/OneWay_Anova_with_TukeyHSD/). The error bars indicate the
489 standard error of the mean (SEM).

490 **ACKNOWLEDGEMENTS**

491 The authors acknowledge Ching-Hong Yang for providing *Dickeya dadantii* 3937
492 strains, which were imported under the permit 106-B-003 issued by the Council of
493 Agriculture of Taiwan. We would like to thank the former and current Lai lab
494 members for their help and fruitful discussion throughout this study, as well as See-
495 Yeun Ting and Mao-Sen Liu for critically reading the manuscript and their valuable
496 comments. We also thank Venus Marie Gaela and Thomas Boudier for the guidance
497 and help in processing the images using Fiji and the Sanger DNA sequencing
498 service provided by Genomic Technology Core located at the Institute of Plant and
499 Microbial Biology, Academia Sinica. The funding was supported by grants National
500 Science and Technology Council (NSTC) of Taiwan (107-2311-B-001-019-MY3) and
501 Academia Sinica Investigator Award (AS-IA-107-L01) to EML, and NSTC grant (110-
502 2311-B001-011) to YLS. YWC was supported by the postdoctoral fellowship (NSTC
503 110-2811-B-001-504). The funders had no role in study design, data collection and
504 interpretation, or the decision to submit the work for publication.

505 **AUTHOR CONTRIBUTION**

506 Conceptualization: MNMS, EML; Investigation: MNMS, KP, PYH, YWC, LKS, YLS,
507 EML; Project Funding acquisition and administration: EML, YLS; Supervision: EML,
508 YLS; Writing of original draft: MNMS, EML; Writing – methodology, review & editing:
509 MNMS, KP, PYH, YWC, LKS, YLS, EML.

510 **FIGURE LEGENDS**

511 **Fig 1. V2c is a PAAR-linked specialized effector containing C-terminal Tox-SHH**
512 **motif. (A)** Schematic diagram of V2c protein showing N-terminal DUF4150 PAAR
513 region and the catalytic region (amino acid 380-409) which covers the Tox-SHH motif.
514 **(B)** Partial sequence alignment of orthologs of V2c from BLASTP. The strain name
515 and accession number are indicated on the left. SHH motif is highlighted in yellow,
516 H383 in red as the metal ion coordinating residue, H384 and H408 of HNH motif for
517 catalysis and metal ion binding, respectively shown in green targeted for mutagenesis
518 are indicated. **(C)** Domain architectures of V2c orthologs, Tox-SHH-containing
519 proteins found in this study. Full length sequences were analyzed and the domains
520 were from Pfam database with E value threshold set at 10^{-5}. **(D)** Cartoon model of V2c
521 (residue 380 – 409). The structure of V2c predicted by AlphaFold indicates V2c
522 consisting a His-Me finger domain with two antiparallel β-strands (yellow) connected
523 with an Ω loop (light blue), a histidine (H384) at the C-terminus of the first β-strand and
524 followed by an α-helix (magenta). The confidence score of this region is higher than
525 90, indicating high structure accuracy.
526

527 **Fig 2. V2c exhibits DNase activity *in vivo* and *in vitro.* (A)** Growth inhibition analysis
528 of expression of *v2c,* its variants, with or without *v3c* encoding putative immunity
529 protein in *E. coli* DH10B. *E. coli* cultures were induced with 1 mM IPTG at 0 h for *v3c*
530 expressed from pTrc200 plasmid followed by L-arabinose (Ara) induction at 1 h to
531 induce *v2c* from pJN105 plasmid. Cell growth was recorded every hour at OD_{600}.
532 Empty vectors (vectors) were used as control. Data are mean ± SEM from four
533 independent experiments. **(B)** Number of colony forming unit (log_{10} CFU/mL)
534 quantified after growth inhibition assay (8 h) in each sample grown on agar plates.
535 Data represents mean ± SEM of four independent experiments. Different letters above
536 the bar indicate statistically different groups of strains ($P < 0.05$) determined by
537 Tukey's HSD test. **(C)** Plasmid degradation assay performed by *E. coli* DH10B cells
538 harboring pTrc200 and pJN105 plasmid (vector) or derivatives expressing *v2c* or its
539 variants with pTrc200, *v2c* or its variants with pTrc200 expressing *v3c* were induced
540 with (+) or without (–) Ara for 2 h. Plasmid DNA was extracted and the degradation
541 pattern was observed in agarose gel. Result shown is a representative data from three

542 independent experiments. **(D)** *In vitro* DNase activity assay performed by using
543 pTrc200HA plasmid DNA as DNA substrate and incubated with purified V2c or its
544 variants. Nuclease free water (ddH_2O), protein elution buffer (elution buffer) and eluate
545 from empty vector expression (pET28a) served as negative controls while Benzonase
546 nuclease served as a positive control. The digestion of DNA substrate was determined
547 by agarose gel electrophoresis. The reaction samples of V2c or its variants were
548 detected by western blotting using anti-V2c antibody (α-V2c).
549
550 **Fig 3. V2c-dependent cellular phenotypes. (A)** Images of *E. coli* DH10B cells
551 harboring vector(s) and its derivatives expressing *v2c* or its variants in the presence
552 or absence of its cognate immunity gene *v3c* with (+Ara) and without (-Ara) Arabinose
553 induction stained with FM4-64 (red) and Hoechst stain (blue). The micrographs from
554 left to right are FM4-64, Hoechst, phase contrast and a merged image of FM-4-64 and
555 Hoechst stains. Scale bar, 2 μm. Two representative images from two independent
556 experiments are shown. **(B)** Normalized Hoechst intensity (intensity/unit area of cells)
557 in different treatments and **(C)** Cell length (μm) as measured from the indicated
558 number of cells (n) per treatment. The graph shows a combined count from 12 frames,
559 with three from each of four independent experiments. The red line in (C) shows the
560 median with interquartile range. Data represents mean ± SEM of four independent
561 experiments. Different letters above the bar indicate statistically different groups of
562 strains ($P < 0.05$) determined by Tukey's HSD test.
563
564 **Fig 4. V2a Tox-AHH DNase exhibits cell elongation phenotype. (A)** Cartoon model
565 of V2a (residue 380 – 470). The structure of V2a predicted by AlphaFold indicates V2a
566 consisting a His-Me finger domain with its signature antiparallel β-strands (yellow)
567 connected with an Ω loop (light blue) with a histidine (H386, orange) at the C-terminus
568 of the first β-strand. Two α-helices (pink) with histidine residues (H430, H456 magenta)
569 followed the β-strands. N412 is found in the loop between the β-strands and H430 is
570 in the first α-helix (E429–G430). The predicted Local-Distance Difference Test
571 (pLDDTs) of the His-Me domains of V2a are from confident to very high, most of the
572 pLDDTs of the residues are > 90. **(B)** Morphological analysis of *E. coli* DH10B cells
573 harboring vector(s) and its derivatives expressing *v2a*, catalytic site (H385A) mutant
574 without (-Ara) and with (+Ara) arabinose induction. Cells were stained with FM4-64
575 (red) and Hoechst stain (blue). The micrographs from left to right are FM4-64, Hoechst,

576 phase contrast and a merged image of the two fluorescent images. Scale bar, 2 μm.
577 **(C)** Cell length (μm) and **(D)** Hoechst intensity in different treatments as determined
578 from a combined count of three random frames, the number of cells (n) per sample is
579 indicated. The graph shows a representative result of three independent experiments.
580 The red line shows the median with interquartile range Different letters above the bar
581 indicate statistically different groups of strains ($P < 0.05$) determined by Tukey's HSD
582 test.
583
584 **Fig 5. Interbacterial competition with *D. dadantii*. (A)** Fluorescence micrographs of
585 1D1609 WT::TssB-sfGFP and Δ*4*::TssB-sfGFP co-cultures against *D. dadantii* 3937
586 WT and Δ*imp* mutant. A representative area selected from several random fields is
587 shown. **(B)** Fluorescence micrographs of *D. dadantii* Δ*imp*-GFP(S65T) and 1D1609 EI
588 pair mutants' co-cultures, at 1:10 ratio, observed after 16h on AK agar. *D. dadantii*
589 Δ*imp*-GFP(S65T) indicated as Dd only is included as a control. The inset in phase
590 contrast shows a magnified image of cells in the red box. White arrows point to *D.*
591 *dadantii* cells. Scale bar, 2 μm. **(C)** Survival of target strains *D. dadantii* 3937 Δ*imp*-
592 GFP(S65T) harboring pRL662 plasmid (Gm^R) mixed at 1:10 ratio with the attacker
593 1D1609 EI mutant strains on the x axis. Surviving *D. dadantii* 3937 were quantified by
594 CFU. The attacker and target strains were spotted on AK agar plates. After 18h, the
595 co-culture was collected, serially diluted and spotted on LB agar plate containing Gm
596 to count the CFU. Data are mean ± SEM (n = 6 biological repeats from three
597 independent experiments). **(D)** Cell length after competition between *A. tumefaciens*
598 1D1609 EI mutants with *D. dadantii* 3937 Δ*imp*-GFP(S65T). Cell length of *D. dadantii*
599 was measured using Fiji analyze particles tool. Data are mean ± SEM (n=6 biological
600 repeats from three independent experiments).
601
602
603 **Fig S1. (A)** Schematic diagram of V4b. The Rhs domain is bordered by conserved
604 motifs. The CT is the C-terminal domain that encodes the putative toxin. **(B)** *E. coli*
605 growth inhibition analysis in *vgrGb*-associated EI pair. *E. coli* cultures were induced
606 with 1 mM IPTG at 0 h for the expression of putative immunity protein expressed on
607 pTrc200 plasmid followed by L-arabinose (Ara) induction at 1 h to induce putative toxin
608 gene from pJN105 plasmid. Cell growth was recorded every hour at OD_{600}. Empty
609 vector was used as control. Data are mean ± SEM of three independent experiments.

610 **(C)** Plasmid degradation assay performed by using full length V4b (*v4b*^{FL}) and C-
611 terminal domain only (*v4b*^{CT}). *E. coli* cells with pTrc200 and pJN105 plasmid (vector)
612 or expressing *v4b* and *v4b*+*v5b* were induced with (+) or without (-) arabinose (Ara)
613 for 2 h. Plasmid DNA was extracted and the degradation pattern was observed in
614 agarose gel. Result shown is a representative data from two independent experiments.
615 **(D)** Images of *E. coli* DH10B cells expressing *v4b* and *v4b* co-expressed with its
616 cognate immunity gene *v5b* (*v4b*+*v5b*) under condition with (+Ara) and without (-Ara)
617 arabinose induction. *E. coli* DH10B cells expressing empty vector (vector) under
618 condition with (+Ara) and without (-Ara) arabinose induction served as negative control.
619 Cells were stained with FM4-64 (red) and Hoechst stain (blue). The micrographs from
620 left to right are FM4-64, Hoechst, phase contrast and a merged image of the two
621 fluorescent micrographs. Two representative images from independent experiments
622 are shown. Scale bar, 2 μm. **(E)** Cell length (μm) as measured from the indicated
623 number of cells (n) per sample. The graph shows a combined count from 3 random
624 frames as a representative of two independent experiments. The red line shows the
625 median with interquartile range. **(F)** Hoechst intensity in cells analyzed in (D). Result
626 shown is a representative data of two independent experiments. Different letters above
627 the bar indicate statistically different groups of strains ($P < 0.05$) determined by
628 Tukey's HSD test.
629
630 **Fig S2. (A)** Representative fluorescence micrographs of *A. tumefaciens* 1D1609
631 (1D1609WT::TssB-sfGFP) and quadruple *vgrG* deletion mutant- (1D1609Δ4::TssB-
632 sfGFP) expressing TssB-sfGFP from the native *tssB* locus (Movie S1). No sheath
633 assembly was observed in 1D1609Δ4::TssB-sfGFP during four min time-lapse
634 observation period. Scale bar: 2 μm. **(B)** Western blot analysis of 1D1609WT::TssB-
635 sfGFP and 1D1609Δ4::TssB-sfGFP. The strains were grown in AB-MES (pH5.5). The
636 cellular and secreted (S) fractions were subjected to immunoblotting probed with
637 antibodies as indicated. Molecular weight markers (in kDa) are indicated on the left,
638 TssB is about 19 kDa while GFP is 27 kDa, resulting 46-kDa TssB-GFP fusion protein.
639 The T6SS inactive mutant Δ*4*Δ*tssB* served as a negative control. Similar results were
640 obtained from two independent experiments.
641
642 **Fig S3.** Cell length (μm) of **(A)** *v2c* single catalytic site mutants and **(B)** catalytic
643 variants co-expressed with *v3c*. Cell length (μm) as measured from the indicated

644 number of cells (n) per sample. The graph shows a combined count from six random
645 frames. Data represents mean ± SEM of four independent experiments. Different
646 letters above the bar indicate statistically different group of strains ($P < 0.05$)
647 determined by Tukey's HSD test. The red line shows the median with interquartile
648 range.
649
650 **Fig S4.** Sequence alignment of V2a and V2c. The conserved amino acid residues are
651 indicated as '∗' (identical), ':' (similar) and '.' (slightly similar). The DUF4150, PAAR-
652 like domain is in green. The histidine residues in AHH and SHH motifs in His-Me finger
653 domain of V2a and V2c respectively, V2aH385/V2cH383 and V2aH386/V2cH384, are
654 in red. The histidine residues that predicted to responsible for metal binding in His-Me
655 finger domain, V2aH430/V2cH408, are in a bold blue font. Two peptides used for
656 generating antibodies were underlined.

657 **SUPPLEMENTARY VIDEO**

658 **Video S1**. Time-lapse recording of *A. tumefaciens* 1D1609 cells expressing TssB-
659 sfGFP from the native *tssB* locus (WT::TssB-sfGFP) showing the full cycle of T6SS
660 assembly: sheath initiation, extension, contraction and disassembly, visualized in less
661 than ~75 s. Up to three visible structures were observed in a single cell and the sheath
662 spreads throughout the width and length of the cell. T6SS machine cycle from one
663 location in the cell to another location.
664
665 Supplementary Table S1. Bacterial strain and plasmids used in this study
666
667 Supplementary Table S2. Primers used in this study

668 **REFERENCES**

669 1. Brackmann M, Nazarov S, Wang J, Basler M. Using Force to Punch Holes: Mechanics
670 of Contractile Nanomachines. Trends in Cell Biology. 2017;27(9):623-32.
671 2. Shneider MM, Buth SA, Ho BT, Basler M, Mekalanos JJ, Leiman PG. PAAR-repeat
672 proteins sharpen and diversify the type VI secretion system spike. Nature.
673 2013;500(7462):350-3.
674 3. Basler M, Pilhofer M, Henderson GP, Jensen GJ, Mekalanos JJ. Type VI secretion
675 requires a dynamic contractile phage tail-like structure. Nature. 2012;483(7388):182-6.
676 4. Cianfanelli FR, Monlezun L, Coulthurst SJ. Aim, Load, Fire: The Type VI Secretion
677 System, a Bacterial Nanoweapon. Trends in Microbiology. 2016;24(1):51-62.
678 5. Coulthurst S. The Type VI secretion system: a versatile bacterial weapon.
679 Microbiology. 2019;165(5):503-15.
680 6. Hwang HH, Yu M, Lai EM. *Agrobacterium*-mediated plant transformation: biology and
681 applications. Arabidopsis Book. 2017;15:e0186.
682 7. Wu CF, Santos MNM, Cho ST, Chang HH, Tsai YM, Smith DA, Kuo CH, Chang JH, Lai EM.
683 Plant pathogenic *Agrobacterium tumefaciens* strains have diverse type VI effector-immunity
684 pairs and vary in in planta competitiveness. Molecular Plant-Microbe Interactions. 2019;
685 32(8).
686 8. Lin C, Lin YC, Haryono M, Santos MNM, Cho ST, Weisberg A, Wu CF, Chang J, Lai EM,
687 Kuo CH. Modular evolution of secretion systems and virulence plasmids in a bacterial species
688 complex. BMC Biology. 2022; 20:16.
689 9. Santos MNM, Cho ST, Wu CF, Chang CJ, Kuo CH, Lai EM. Redundancy and Specificity
690 of Type VI Secretion *vgrG* Loci in Antibacterial Activity of *Agrobacterium tumefaciens* 1D1609
691 Strain. Frontiers in Microbiology. 2019;10(3004):3004.
692 10. Jablonska J, Matelska D, Steczkiewicz K, Ginalski K. Systematic classification of the His-Me
693 finger superfamily. Nucleic Acids Research. 2017;45(20):11479-94.
694 11. Zhang D, de Souza RF, Anantharaman V, Iyer LM, Aravind L. Polymorphic toxin systems:
695 Comprehensive characterization of trafficking modes, processing, mechanisms of action,
696 immunity and ecology using comparative genomics. Biology Direct. 2012;7(1):18.
697 12. Wu CC, Lin LJ and Yuan HS. Structures, Mechanisms, and Functions of His-Me Finger
698 Nucleases. Trends in Biochemical Sciences. 2020;45(11):935-946.

699 13. Zhang D, Iyer LM, Aravind L. A novel immunity system for bacterial nucleic acid
700 degrading toxins and its recruitment in various eukaryotic and DNA viral systems. Nucleic
701 Acids Research. 2011;39(11):4532-52.
702 14. Jana B, Fridman CM, Bosis E, Salomon D. 2019. A modular effector with a DNase
703 domain and a marker for T6SS substrates. Nature Communications 10:3595 (2019).
704 15. Söding J, Biegert A, Lupas AN. The HHpred interactive server for protein homology
705 detection and structure prediction. Nucleic Acids Research. 2005;33:W244-W8.
706 16. Wu CF, Lien YW, Bondage D, Lin JS, Pilhofer M, Shih YL, Chang JH, Lai EM. Effector
707 loading onto the VgrG carrier activates type VI secretion system assembly. EMBO Reports.
708 2019; 5:e47961.
709 17. Pissaridou P, Allsopp LP, Wettstadt S, Howard SA, Mavridou DAI, Filloux A. The
710 *Pseudomonas aeruginosa* T6SS-VgrG1b spike is topped by a PAAR protein eliciting DNA
711 damage to bacterial competitors. Proceedings of the National Academy of Sciences of the
712 United States of America. 2018;115(49):12519-24.
713 18. Pei T-T, Li H, Liang X, Wang Z-H, Liu G, Wu L-L, et al. Intramolecular chaperone-mediated
714 secretion of an Rhs effector toxin by a type VI secretion system. Nature Communications.
715 2020;11(1):1865.
716 19. Fridman CM, Jana B, Ben-Yaakov R, Bosis E, Salomon D. A DNase Type VI Secretion
717 System Effector Requires Its MIX Domain for Secretion. Microbiology Spectrum.
718 2022;13:e0246522.
719 20. Bernal P, Allsopp LP, Filloux A, Llamas MA. The *Pseudomonas putida* T6SS is a plant
720 warden against phytopathogens. ISME Journal. 2017;11(4):972-987.
721 21. Li Y, Yan X, Tao Z. Two Type VI Secretion DNase Effectors are Utilized for Interbacterial
722 Competition in the Fish Pathogen *Pseudomonas plecoglossicida*. Frontiers in Microbiology.
723 2022;13:869278.
724 22. Wu C-C, Lin JLJ, Yuan HS. Structures, Mechanisms, and Functions of His-Me Finger
725 Nucleases. Trends in Biochemical Sciences. 2020;45(11):935-46.
726 23. Galburt EA, Chevalier B, Tang W, Jurica MS, Flick KE, Monnat RJ, et al. A novel
727 endonuclease mechanism directly visualized for I-PpoI. Nature Structural Biology.
728 1999;6(12):1096-9.

729 24. Yu M, Wang YC, Huang CJ, Ma LS, Lai EM. *Agrobacterium tumefaciens* deploys a
730 versatile antibacterial strategy to increase its competitiveness. Journal of Bacteriology
731 2021;203(3):e00490-20.
732 25. Ting S-Y, Bosch DE, Mangiameli SM, Radey MC, Huang S, Park Y-J, et al. Bifunctional
733 Immunity Proteins Protect Bacteria against FtsZ-Targeting ADP-Ribosylating Toxins. Cell.
734 2018;175(5):1380-92.e14.
735 26. Justice SS, Hunstad DA, Cegelski L, Hultgren SJ. Morphological plasticity as a bacterial
736 survival strategy. Nature Reviews Microbiology. 2008;6(2):162-8.
737 27. LaCourse KD, Peterson SB, Kulasekara HD, Radey MC, Kim JY, Mougous JD. Conditional
738 toxicity and synergy drive diversity among antibacterial effectors. Nature Microbiology
739 2018;3:440–446.
740 28. Wu CF, Weisberg AJ, Davis EW 2nd, Chou L, Khan S, Lai EM, Kuo CH, Chang JH.
741 Diversification of the Type VI Secretion System in Agrobacteria. mBio.
742 2021;26;12(5):e0192721.
743 29. Edgar RC. MUSCLE: multiple sequence alignment with high accuracy and high throughput.
744 Nucleic Acids Res. 2004;32(5):1792-7.
745 30. Mistry J, Chuguransky S, Williams L, Qureshi M, Salazar Gustavo A, Sonnhammer ELL, et
746 al. Pfam: The protein families database in 2021. Nucleic Acids Research. 2021;49(D1):D412-
747 D9.
748 31. Ma L-S, Hachani A, Lin J-S, Filloux A, Lai E-M. *Agrobacterium tumefaciens* deploys a
749 superfamily of type VI secretion DNase effectors as weapons for interbacterial competition in
750 planta. Cell Host Microbe. 2014;16(1):94-104.
751 32. Schindelin J, Arganda-Carreras I, Frise E, Kaynig V, Longair M, Pietzsch T, et al. Fiji: an open-
752 source platform for biological-image analysis. Nature Methods. 2012;9(7):676-82.

Fig 1. Domain and sequence analysis of V2c.

(A)

(B)

```
Agrobacterium tumefaciens 1D1609                AVH44366.1       -NLDSHHTPANS---A--SYLPTWAG-----PAIQMLPEDHR  409
Silvanigrella aquatica 1915309#                 WP_148696535.1   -GLDSHHMPAKS---AYEGSKMNPDGEAKQGPAIKMEPKDHR  268
S. enterica serovar Enteritidis IVB 176/82*     HAU6875067.1     -GLDSHHMPAKD---S--SPLSHDDG-----PAIHMDPLDHR  149
S. enterica serovar Enteritidis SARB17*         ELO80288.1       -GLDSHHMPAKD---S--SPLSHDDG-----PAIHMDPLDHR  150
Ralstonia solanacearum SEPPX05**                ARU21619.1       -GKDSHHMPADD---V--SPLARNGG-----PAIQMEPKDHK  221
Ralstonia solanacearum 305**                    WP_087451447.1   -GKDSHHMPADD---V--SPLARNGG-----PAIQMEPKDHK  367
Paraburkholderia phosphatilytica 2282883**      WP_124800779.1   -GKDSHHMPADD---A--SPLPKKDG-----PAIQMDPADHH  217
Caballeronia mineralivorans 2010198**           WP_053064266.1   -GKDSHHMPADD---V--SPLKRNDG-----PAIQMEPDDHA  323
Burkholderia vietnamiensis 60552**              WP_196483818.1   -GKDSHHMPADD---V--SPLKRSDG-----PAIQMDPDDHA  227
Burkholderia vietnamiensis 60552**              WP_155626574.1   -GKDSHHMPADD---V--SPLKRSDG-----PAIQMDPDDHA  243
Burkholderia cenocepacia 95486**                WP_200039262.1   -GKDSHHMPADD---V--SPLKRSDG-----PAIQMDPDDHA  243
Burkholderia anthina 179879**                   WP_155634575.1   -GKDSHHMPADD---V--SPLKRSDG-----PAIQMDPDDHA  227
Burkholderia cenocepacia 95486**                WP_124550222.1   -GKDSHHMPADD---V--SPLKRSDG-----PAIQMDPDDHA  243
Massilia armeniaca 2072590**                    WP_181259249.1   -GKDSHHLPADD---V--SPLKRSDG-----PAIQMDPEDHK  236
Herbaspirillum rubrisubalbicans M1**            ALU88908.1       -GKDSHHMPADN---V--SPLKSNEG-----PAIQMDPLDHK  244
Herbaspirillum rubrisubalbicans M1**            ALU90982.1       -GKDSHHMPADD---V--SPLKRNEG-----PAIQMDPLDHK  244
```

(C)

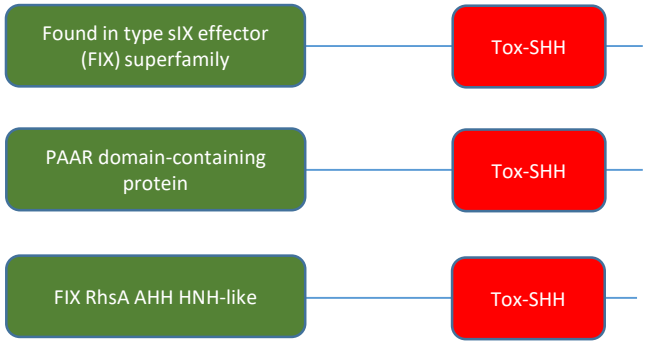

(D)

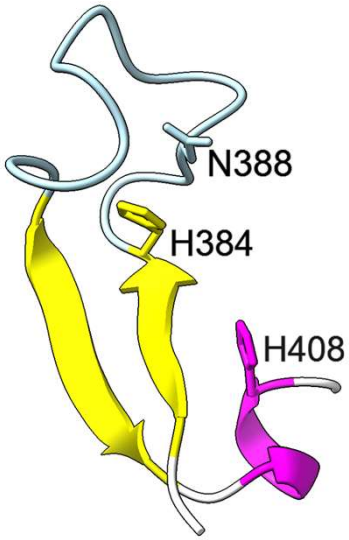

Fig 2. V2c exhibits DNase activity *in vivo* and *in vitro.*

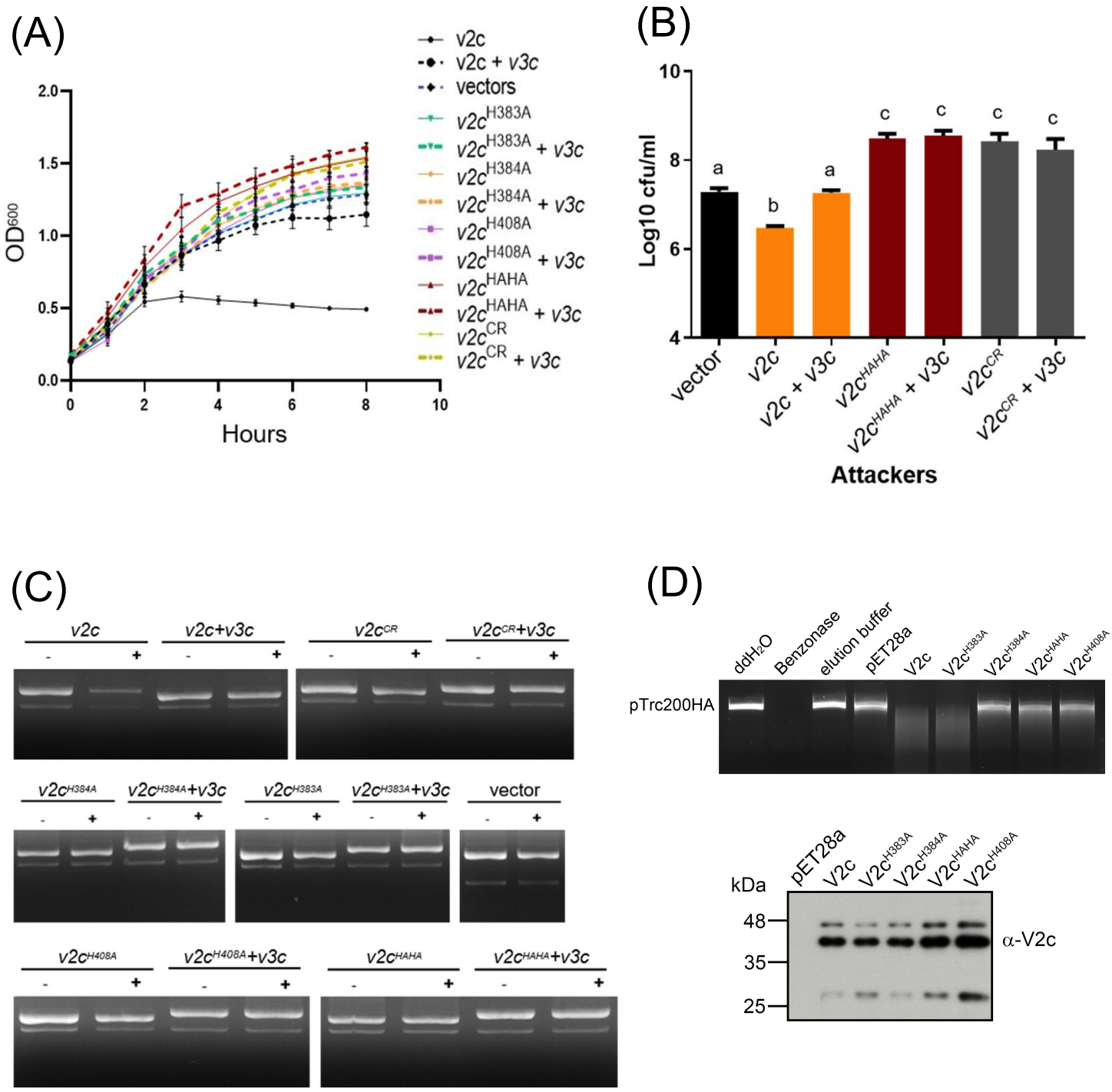

Fig 3. V2c-dependent cellular phenotypes.

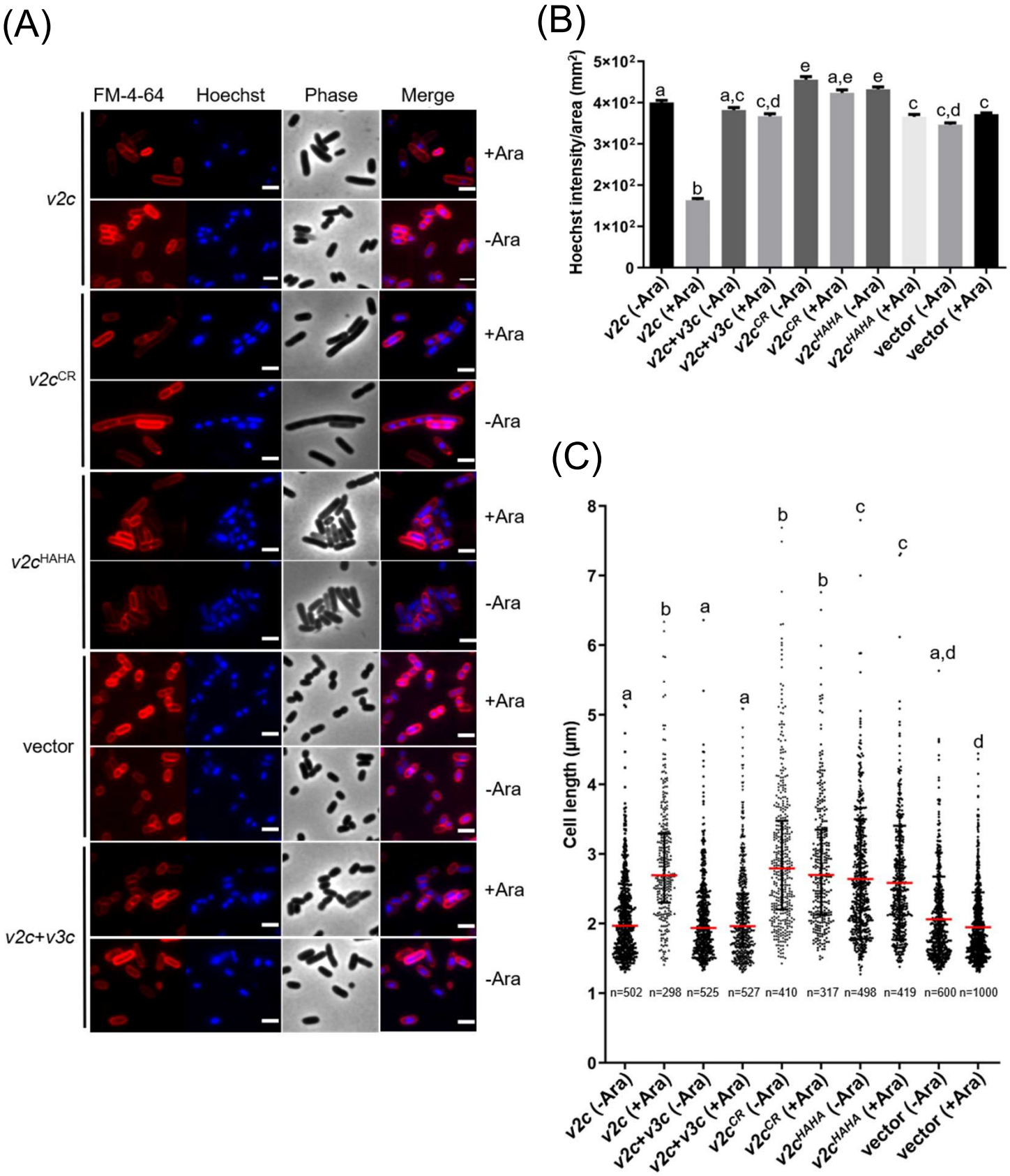

Fig 4. V2a also exhibits cell elongation phenotype.

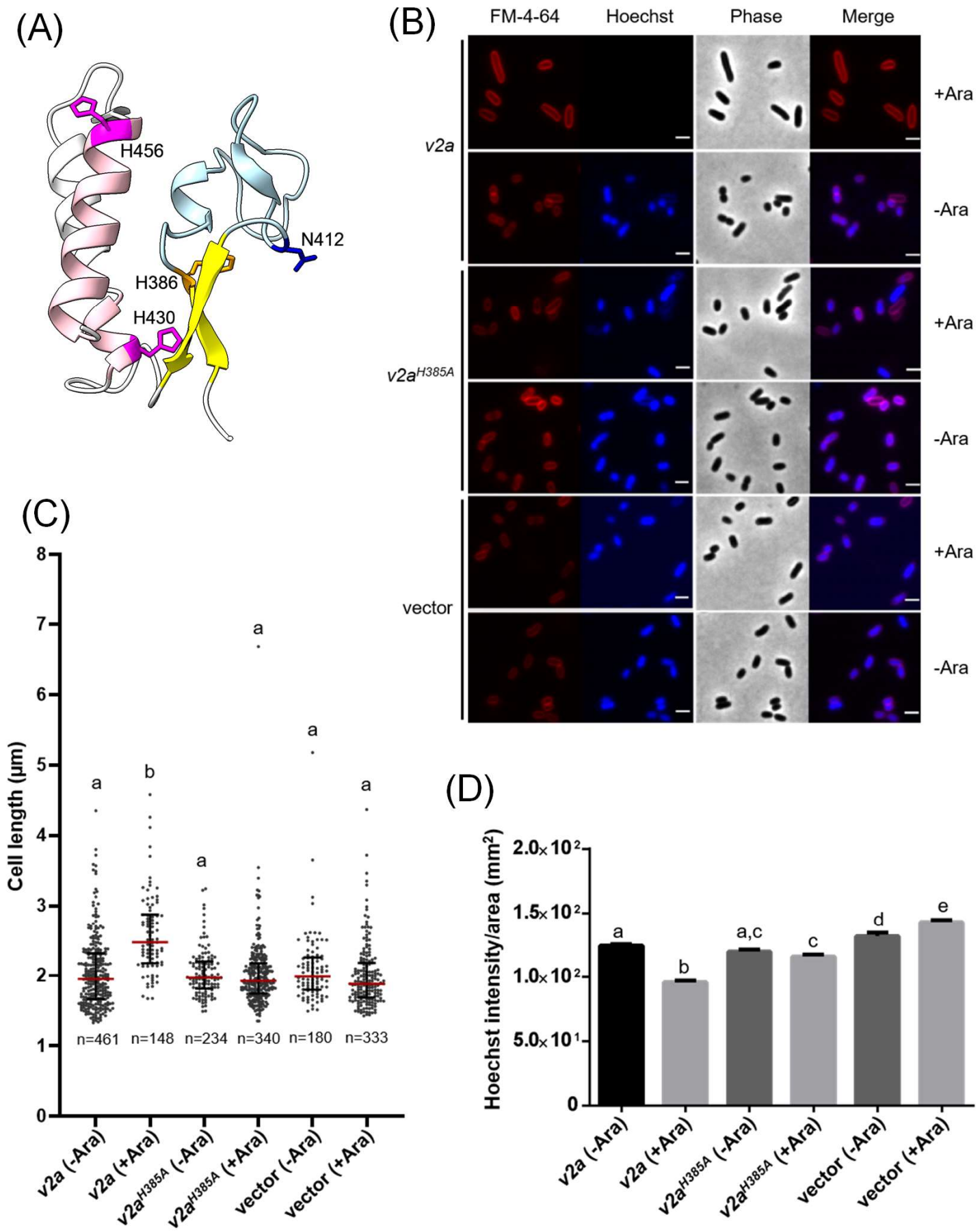

Fig 5. Interbacterial competition with *D. dadantii*.

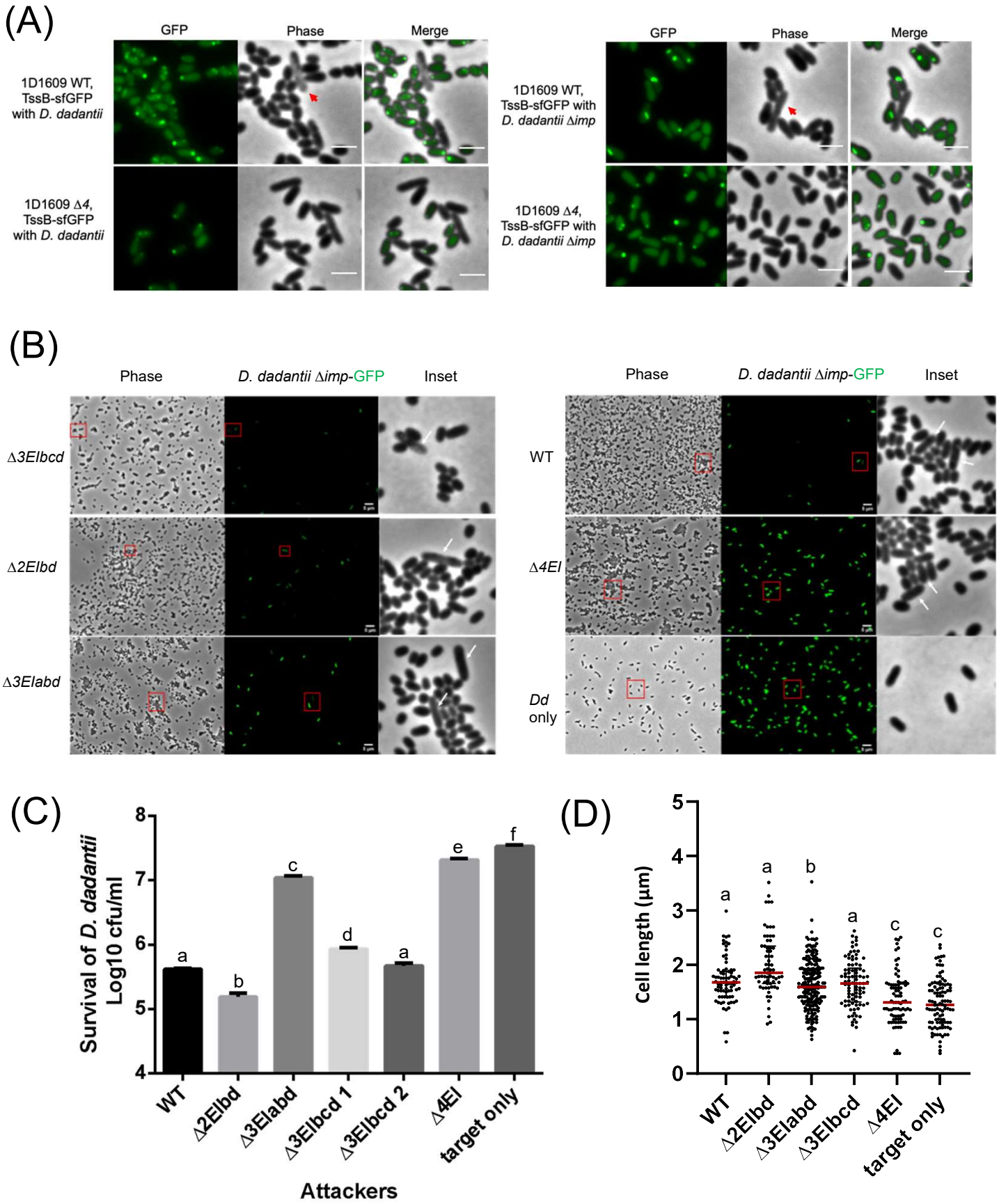

Figure S1.

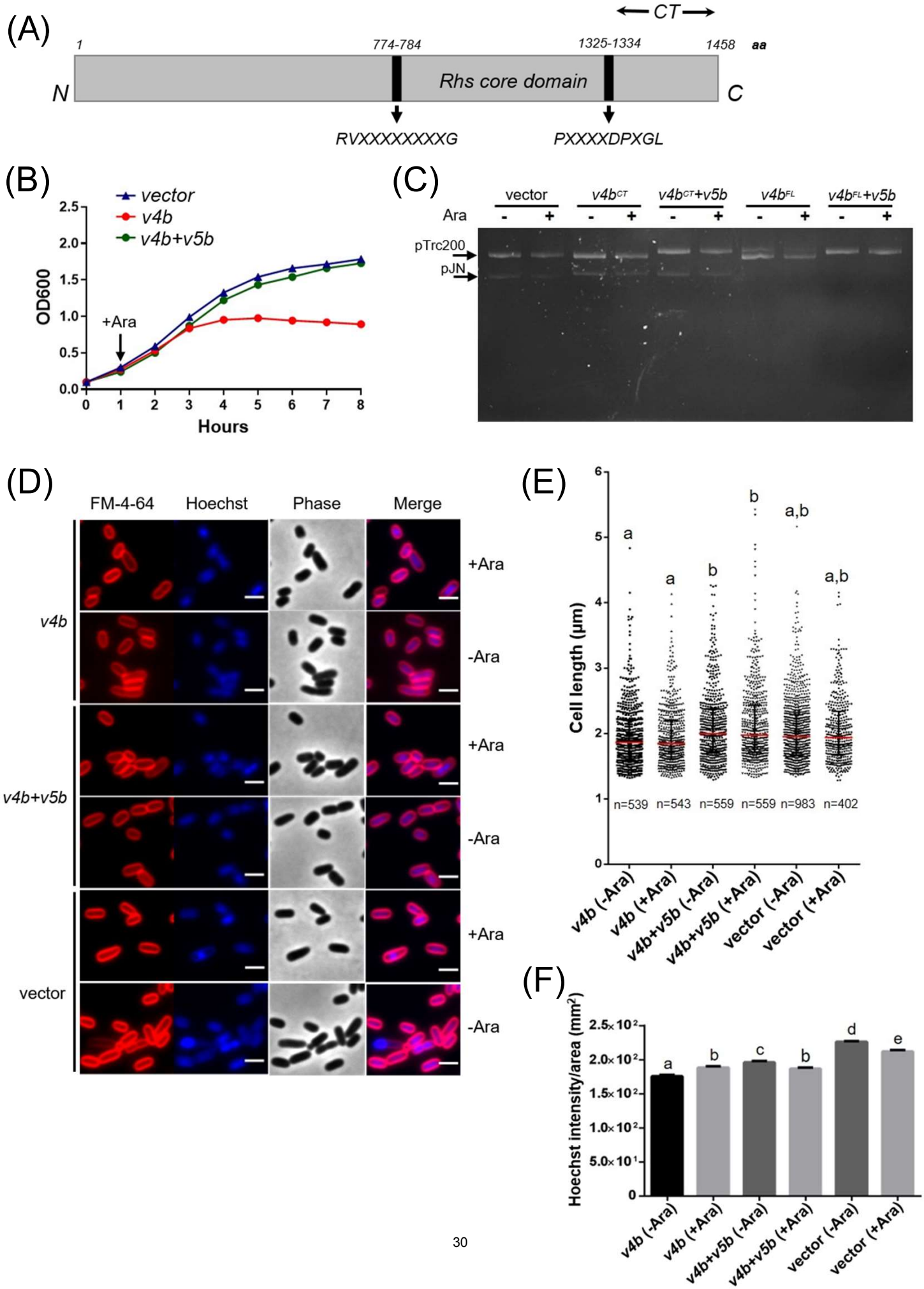
(A)
CT
1
774-784
1325-1334
1458
aa
N
Rhs core domain
C
RVXXXXXXXXG
PXXXXDPXGL
(B)
vector
v4b
v4b+v5b
OD600
+Ara
Hours
(C)
vector
v4bCT
v4bCT+v5b
v4bFL
v4bFL+v5b
Ara
pTrc200
pJN
(D)
FM-4-64
Hoechst
Phase
Merge
v4b
v4b+v5b
vector
+Ara
-Ara
(E)
Cell length (μm)
n=539
n=543
n=559
n=559
n=983
n=402
v4b (-Ara)
v4b (+Ara)
v4b+v5b (-Ara)
v4b+v5b (+Ara)
vector (-Ara)
vector (+Ara)
(F)
Hoechst intensity/area (mm²)
v4b (-Ara)
v4b (+Ara)
v4b+v5b (-Ara)
v4b+v5b (+Ara)
vector (-Ara)
vector (+Ara)

Figure S2

(A)

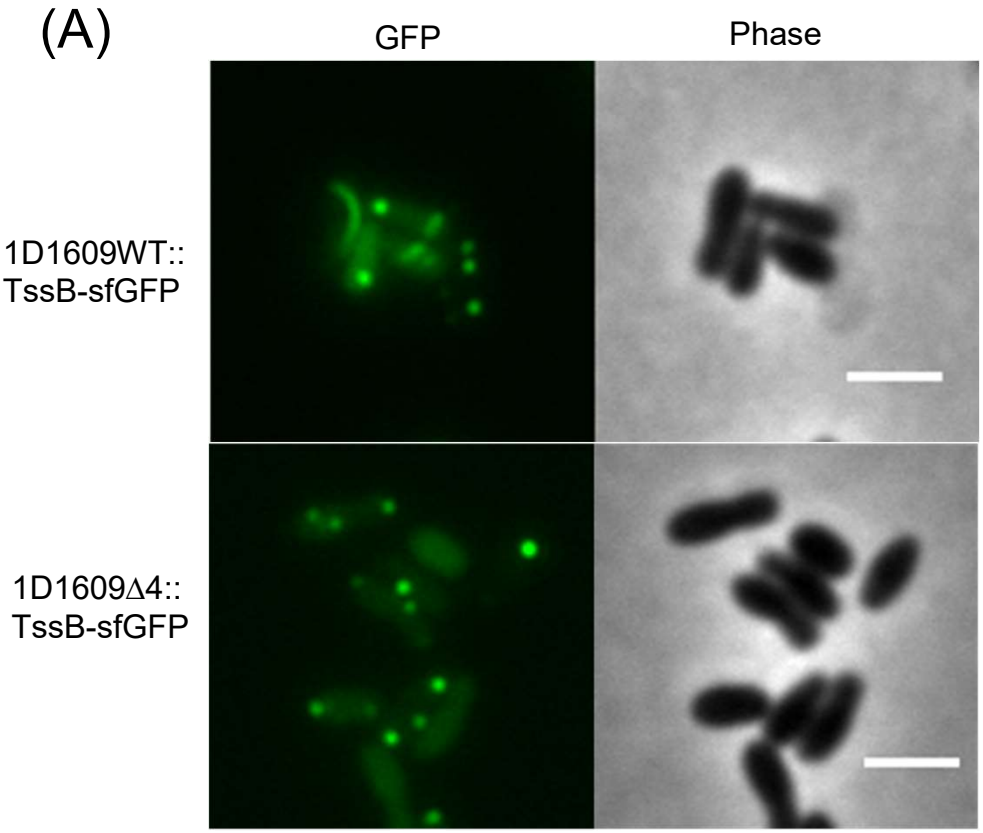
GFP
Phase
1D1609WT::
TssB-sfGFP
1D1609Δ4::
TssB-sfGFP

(B)

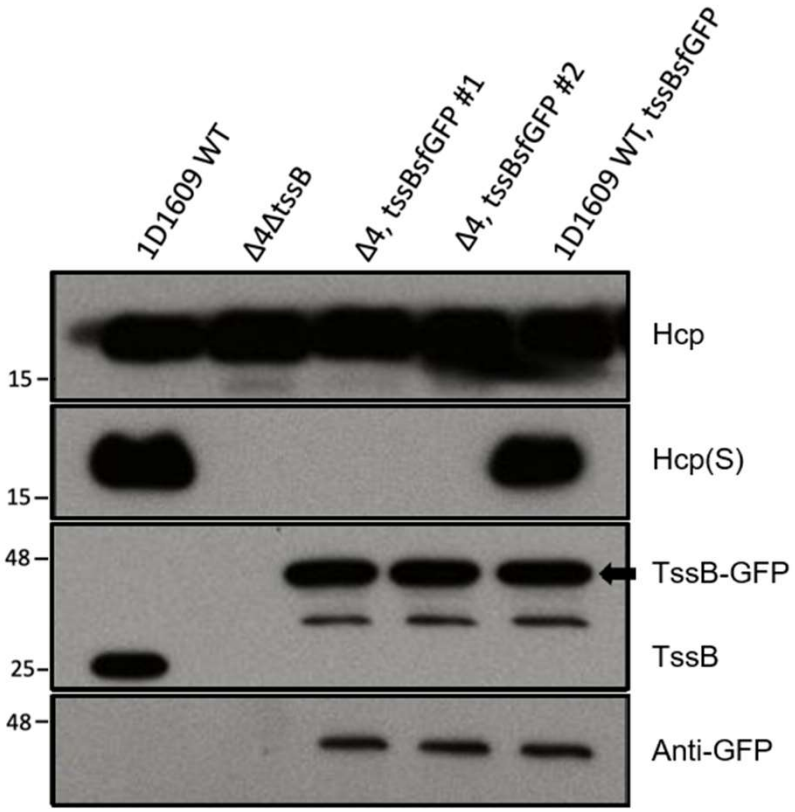
1D1609 WT
Δ4ΔtssB
Δ4, tssBsfGFP #1
Δ4, tssBsfGFP #2
1D1609 WT, tssBsfGFP
Hcp
15
Hcp(S)
15
48
TssB-GFP
TssB
25
48
Anti-GFP

Figure S3

(A)

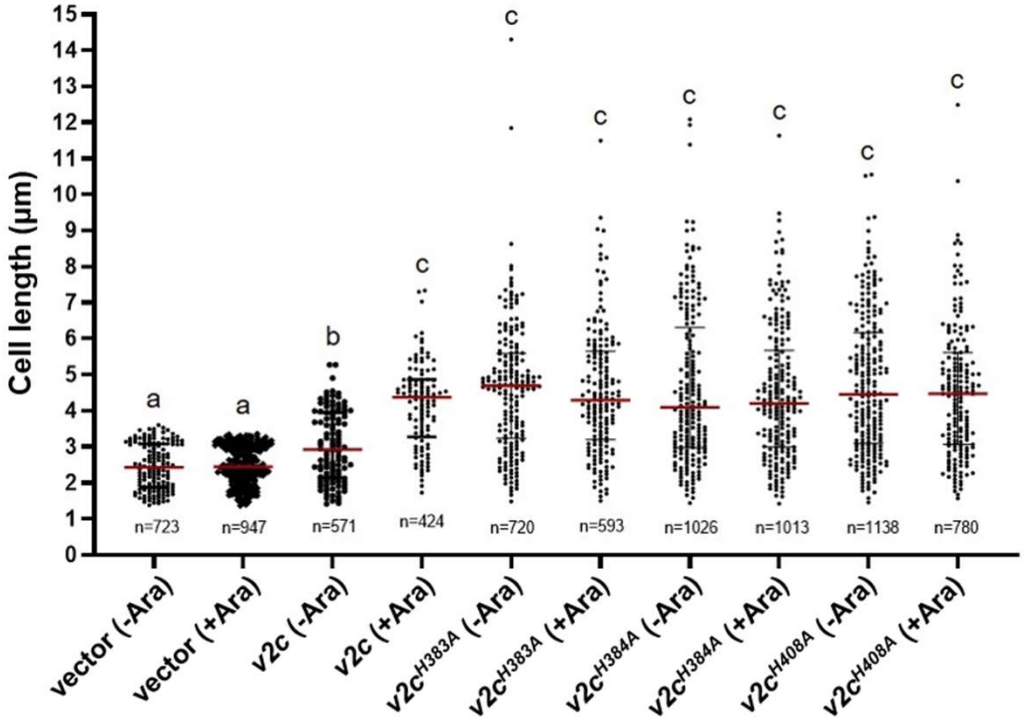
Cell length (µm)
0
1
2
3
4
5
6
7
8
9
10
11
12
13
14
15
a
a
b
c
c
c
c
c
c
c
n=723
n=947
n=571
n=424
n=720
n=593
n=1026
n=1013
n=1138
n=780
vector (-Ara)
vector (+Ara)
v2c (-Ara)
v2c (+Ara)
v2c^{H383A} (-Ara)
v2c^{H383A} (+Ara)
v2c^{H384A} (-Ara)
v2c^{H384A} (+Ara)
v2c^{H408A} (-Ara)
v2c^{H408A} (+Ara)

(B)

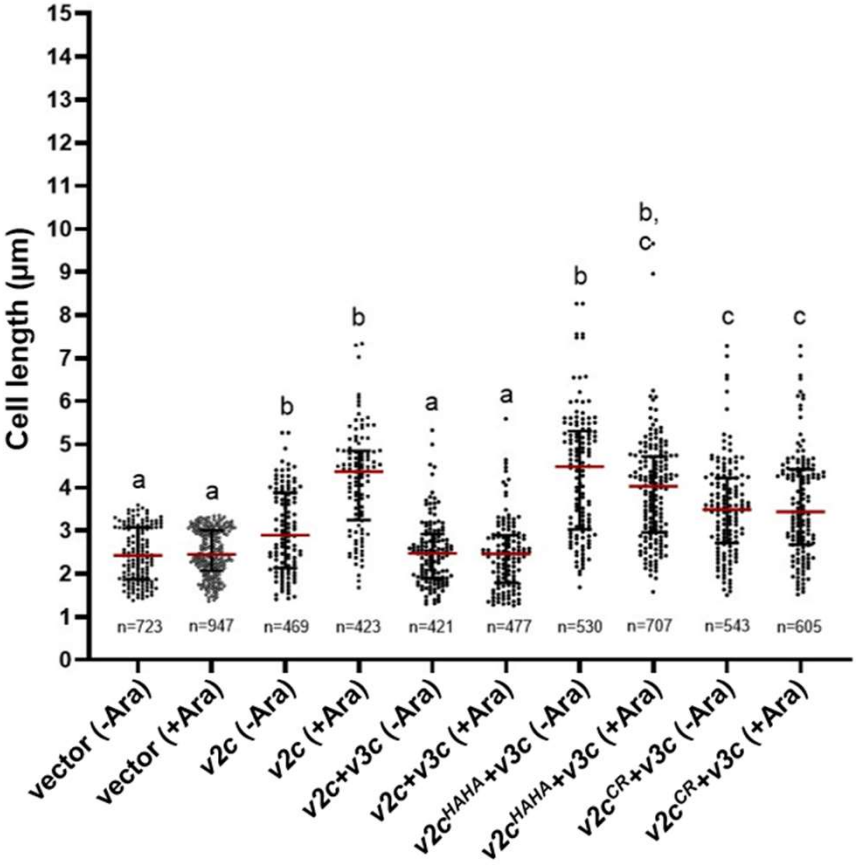
Cell length (µm)
0
1
2
3
4
5
6
7
8
9
10
11
12
13
14
15
a
a
b
b
a
a
b
b, c
c
c
n=723
n=947
n=469
n=423
n=421
n=477
n=530
n=707
n=543
n=605
vector (-Ara)
vector (+Ara)
v2c (-Ara)
v2c (+Ara)
v2c+v3c (-Ara)
v2c+v3c (+Ara)
v2c^{HAHA}+v3c (-Ara)
v2c^{HAHA}+v3c (+Ara)
v2c^{CR}+v3c (-Ara)
v2c^{CR}+v3c (+Ara)

Figure S4.

```
V2a     MSIPRDNYIGEPQYPGTWTTATPREGLRDIDEARIVSLAPDVCLTPVGSSVVPIPYPVVD
V2c     MSIPRDNYIGEPQYPGTWTTATPREGLRDIDEARIVSLAPDVCLTPVGSSVVPIPYPVVD
        ************************************************************
V2a     FCGHDKNYTPSVRFTGKKAMVMRSFTTHVHGDAPGNRKGVKSGTVESICEPIGHADQVRA
V2c     FCGHDKNYTPSVRFTGKKAMVMRSFTTHVHGDAPGNRKGVKSGTVESICEPIGHADQVRA
        ************************************************************
V2a     EGSHVIRHLDRFYMNSRNTQGEAIFVRSTQTYDPPKDDDPVRGSLRWQDGSDEGRVMSDA
V2c     EGSHVIRHLDRFYMNSRNTQGEAIFVRSTQTYDPPKDDDPVRGSLRWQDGSDEGRVMSDA
        ************************************************************
V2a     SPEPFKEGEKYAYAGSAAAATTGAAQNSAQALRGGMPATRPTVPQTVPRGPGRVITPGPA
V2c     SPEPLIMGAQYAQAQTATIPQSGGV-----ARRGTYGRPTTTVDPRLLKGL-RFWSSARG
        ****:  * :** * :*: . :*..     * **    . .**   : .*  *. :.. .
V2a     RAP---QWYRTPPHRVVSDLA-KVG---------RLARVGIWAR-RLNVIGILSSVLIPD
V2c     AAEIMDMVQQISEDRAVQDSAGQLGLNLSDPTDVLVARAHAWSKYHIDASPFYWD--FPN
         *       . .  *.*.* * ::*          :**.  *:. .::.  :  .  :*:
V2a     NGANLSDVVPRDDQERRIKEMFDEGVDAGHDSWEMRDWAMEELRRHRQRVREEPESRPQA
V2c     SQ------VGRDAATKAITSM--EAAAPG----TLGE-ALQGDRTQLEKLRTAIKNAVSA
        .        * **   . *..*  *.. .*     : : *::  * : :.:*   :.  .*
V2a     LPQSETVRVSDRDEYRKKCQVDRYGKMKSVCGQYGMQAHHIVPDWTLRYGAREEADKRIP
V2c     ATAAASVRVSG-----QPCAREALG----APGKYRGGAHFAT---ALPLGDNLDSHHTPA
         . : :****.     : *  :  *    . *:*   **. .   :*  * . :: :  .
V2a     NMPSLNDGMAICVIGNARVEQTEHWGGHLAD------KAIENAGRNSTPPFTAPLHKVVQ
V2c     NSASY----------------LPTWAGPAIQMLPEDHRATLSYGRKVTSPYISTQARLIN
        * .*                   *.*   :      .*  . **: *.*: :.  .:::
V2a     ASAQAMISVRPDCAKEIMAALTTQYAGKNPFQLLRAK--QYPPLPEETISALKSGAVEGA
V2c     SG-------------QFMKAINMDILDIKRIAMLRGDPTRYDAAIAQMMAYAECLKREGI
        :.             ::* *:. :  . : : :**..  .* .   : ::  :.   **
V2a     TRKP
V2c     IK--
         .
```

Supplementary Video 1.

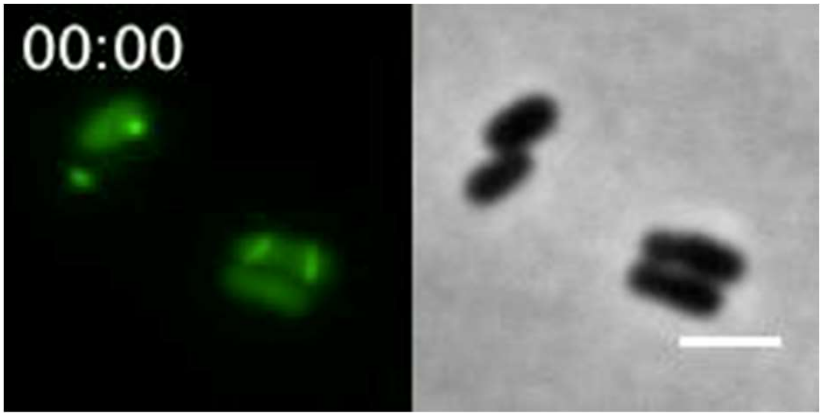

Table S1. Bacterial strains and plasmids

Strain	Relevant characteristics	Reference/Source	EML No.
E. coli			
DH10B	Host of plasmid for cloning	Lab stock	EML455
S17-1	Host for conjugation	Lab stock	EML124
BL21 (DE3)	For protein expression	Lab stock	EML117
***D. dadantii* 3937**			
WT	Wild-type *Dickeya dadantii* 3937	Ching-Hong Yang, University of Wisconsin, Milwaukee	EML4911
Δ*imp*	T6SS inactive strain with deletion of *imp* operon	Ching-Hong Yang, University of Wisconsin, Milwaukee	EML4921
***A. tumefaciens* 1D1609**			
WT	Alfalfa isolate, virulent strain containing pTi1D1609	Clarence Kado, UC Davis	EML304
Δ*4* or Δ*vgrGabcd*	Deletion of *vgrGa*, *vgrGb*, *vgrGc* and *vgrGd*	Santos et al., 2020	EML4746
Δ2*EIbd*	Deletion of *vgrGb*- and *vgrGd*-associated effector-immunity pair	This study	EML5531
Δ3EIbcd #1	Deletion of *vgrGb*-, *vgrGc*- and *vgrGd*-associated effector - immunity pair	This study	EML5594

Δ3EIbcd #2	Deletion of *vgrGb*-, *vgrGc*- and *vgrGd*-associated effector - immunity pair	This study	EML5920
Δ3*EIabd*	Deletion of *vgrGa*-, *vgrGb*- and *vgrGd*-associated effector - immunity pair	Santos et al., 2020	EML5515
Δ4*EIabcd*	Deletion of *vgrGa*-, *vgrGb*- and *vgrGd*-associated effector - immunity pair and whole *vgrGc* cluster (Δ*vgrGc-v3*)	Santos et al., 2020	EML5540
1D1609 WT::TssB-sfGFP	*tssB*-sfGFP integrated into WT chromosome to replace the endogenous *tssB*	This study	EML5559
Δ4::TssB-sfGFP	*tssB*-sfGFP integrated into Δ*4* chromosome to replace the endogenous *tssB*	This study	EML5567

Plasmids			
pJQ200KS	Gm^R, suicide plasmid containing GmR and sacB gene for selection of double crossover	Quandt and Hynes, 1993	EML121
pRL662	Gm^R, broad host range vector derived from pBBR1MCS-2	Vergunst et al., 2000	EML315
pTrc200	Sp^R, pVS1 origin, *lacIq, trc* promoter expression vector	Schmidt-Eisenlohr et al., 1999	EML904

pJN105	Gm^R, arabinose-inducible gene expression vector derived from pBBRMCS-1, *araC*-P_{BAD}	Newman and Fuqua, 1999	EML4220
pET28a	Km^R, Protein expression vector, N-terminal His-tagged	Lab stock	EML2485
pJN-*v2a*	Gm^R, pJN expressing *v2a*	Santos et al., 2020	EML5272
pJN-*v4b*^{FL}	Gm^R, pJN expressing the full-length *v4b*	This study	EML4758
pJN-*v4b*^{CT}	Gm^R, pJN expressing the C-terminal toxin domain of *v4b*	This study	EML4756
pJN-*v2c*	Gm^R, pJN expressing *v2c*	This study	EML5328
pTrc-*v5b*	Sp^R, pTrc200 expressing the immunity protein V5b	This study	EML4759
pTrc-*v3c*	Sp^R, pTrc200 expressing the immunity protein V3c	This study	EML5337
pJN-*v2a* (H385A)	Gm^R, pJN expressing *v2a* with amino acid substitution (H385A)	Santos et al., 2020	EML5298
pJN-*v2c* (H383A)	Gm^R, pJN expressing *v2c* with amino acid substitution (H383A)	This study	EML5925
pJN-*v2c* (H384A)	Gm^R, pJN expressing *v2c* with amino acid substitution (H384A)	This study	EML5926
pJN-*v2c* (H408A)	Gm^R, pJN expressing *v2c* with amino acid substitution (H408A)	This study	EML5927
pJN-*v2c* (HAHA)	Gm^R, pJN expressing *v2c* with amino acid substitution (H383AH384A)	This study	EML5922

pJN-*v2c* CR	Gm^R, pJN expressing *v2c* with deletion of the conserve region of Tox-SSH domain	This study	EML5589
pJQ200sk-*vag4vag5b*	Gm^R, plasmid to generate Δ3*EIbcd* #2	This study	EML5307
pJQ200sk-*vag2vag3d*	Gm^R, plasmid to generate Δ2*EIbd*, Δ3*EIbcd* #1 and Δ3*EIabd*	This study	EML5340
pRL662-GFP(S65T)	GFP from pRU1156 cloned into pRL662	Lab stock	EML3376
pJQ200sk-tssBsfGFP	C-terminal fusion of TssB with superfolder GFP (sfGFP) in pJQ200ks to replace the endogenous *tssB* in WT and Δ*4* background	This study	EML5557
pET28a-*v2c*	pET28a expressing His-tagged V2c	This study	EML6050
pET28a-*v2c*HAHA	pET28a expressing His-tagged V2c H383AH384A	This study	EML6051
pET28a-*v2c*H408A	pET28a expressing His-tagged V2cH408A	This study	EML 6063
pET28a-*v2c*H383A	pET28a expressing His-tagged V2cH383A	This study	EML 6064
pET28a-*v2c*H384A	pET28a expressing His-tagged V2cH384A	This study	EML 6065

Table S2. Primers used in this study

Primer Name	Sequences	Purpose
V2c(H383A)	5'-CCGGAATTCAAGGAACAGCTATGAGCATCCCCCGCGAC-3’ 5'- GACAATTTAGATAGCGCGCATACTCCTGCTAACTCT-3' 5'- AGAGTTAGCAGGAGTATGCGCGCTATCTAAATTGTC-3' 5'- CGTCTAGATCACTTTATGATTCCTTCGCG-3'	mutagenesis
V2c(H384A)	5'-CCGGAATTCAAGGAACAGCTATGAGCATCCCCCGCGAC-3’ 5'-GACAATTTAGATAGCCATGCGACTCCTGCTAACTCT-3' 5'-AGAGTTAGCAGGAGTCGCATGGCTATCTAAATTGTC-3' 5'- CGTCTAGATCACTTTATGATTCCTTCGCG-3'	mutagenesis
V2c(H408A)	5'-CCGGAATTCAAGGAACAGCTATGAGCATCCCCCGCGAC-3’ 5'- ATGCTTCCAGAAGACGCGCGAGCTACACTCTCATAT -3' 5'-TGAGAGTGTAGCTCGCGCGTCTTCTGGAAGCAT-3' 5'- CGTCTAGATCACTTTATGATTCCTTCGCG-3'	mutagenesis
V2c(CR)	5'-GTTTTTTTGGGCTAGCGAAGGAACAGCTATGAGCATC-3’ 5'-CCTTTCTTCCATATGAGAGTGTAGCATTGTCGCCAAGTGGGAGGGCCGTC-3' 5'-GACGGCCCTCCCACTTGGCGACAATGCTACACTCTCATATGGAAGAAAGG -3' 5'-GCGGTGGCGGCCGCTTCACTTTATGATTCCTTCGC-3'	mutagenesis
V2c(H383A H384A)	5'-CCGGAATTCAAGGAACAGCTATGAGCATCCCCCGCGAC-3’ 5'-GACAATTTAGATAGCCATGCGACTCCTGCTAACTCT-3' 5'-AGAGTTAGCAGGAGTCGCATGGCTATCTAAATTGTC-3' 5'- CGTCTAGATCACTTTATGATTCCTTCGCG-3'	mutagenesis
pJQ200KS-*v4bv5b*	5'-TTTCTAGACATCTGTTGTTCGCGGCCGATG-3’ 5'-GCGGATCCATCACCCGCCATGTGAGGCCT-3' 5'-GCGGATCCTTCGCTGCCCTGTGACCGTTCT-3' 5'-GCCCCGGGGCAAGATGATTCCGGGAATTGAC-3'	deletion mutant
pJQ200KS-v2dv3d	5'-GCTCTAGAGAGCGCCGAAATCCGCTT-3' 5'-CGGGATCCGATGCTCATGCTGTCTCCCTCTC-3' 5'-CGGGATCCGCCAGAAAGCCATAGATTGTCG-3' 5'-TCCCCCCGGGGCATCACCACACTCTCGAGCCT-3'	deletion mutant

V4b	5'-CCGTCTAGAAAGGAACAGCTATGGCGGGTGAT-3' 5'-CGGAGCTCGTTTCGATACTCAGCATCGACCG-3'	overexpression
V5b	5'-TATAGGTACCCGAGAATAAGAACCGCGTTC-3' 5'-GCTCTAGAATTGGCGAGGCTACAGCG-3'	overexpression
V2c	5'-CCGGAATTCAAGGAACAGCTATGAGCATCCCCCGCGACAATTAT-3' 5'-CGTCTAGATCACTTTATGATTCCTTCGCGTTTAAGGC-3'	overexpression
V3c	5'-ATCCGAGCTCGTGACAGACAAGTCGGGAGCG-3' 5'-GCTCTAGACCTAGATCCATCGCTTACTGCCTC-3'	overexpression
tssB-sfGFP	UF 5'-TTTCTAGACGAGCTTCGACGCCATCATGGCGG-3' UR 5'-TTTGCTCGCGCCGTTCTTTTCCTT-3' sfGFP F 5'-CAAGGAAAAGAACGGCGCGAGCAAAATGCGTAAAGGCGAAGAGCTGTTCA-3' sfGFP R 5'-GGGAGGTTTTCCTCCGCACAGGCGATCATTTGTACAGTTCATCCATACCA-3' DF 5'-TGGTAGGGATGAACTGTACAAATGATCGCCTGTGCGGAGGAAAACCTCCC-3' DR 5'-TCCCCCCGGGCAGCTGTACGTCATCGAAGGAA-3'	Chromosomal replacement
pET28a-v2c	5'-AATCTAGAATGAGCATCCCCCGCGACAA-3'. 5'-AACTCGAGCTTTATGATTCCTTCGC-3'	Protein expression
pET28a-v2cHAHA	5'-GACAATTTAGATAGCGCGGCGACTCCTGCTAACTCT-3'. 5'-AGAGTTAGCAGGAGTCGCCGCGCTATCTAAATTGTC-3'	Protein expression
pET28a-v2c-H383A	5'-GACAATTTAGATAGCGCGCATACTCCTGCTAACTCT-3' 5'-AGAGTTAGCAGGAGTATGCGCGCTATCTAAATTGTC-3'	Protein expression
pET28a-v2c-H384A	5'-GACAATTTAGATAGCCATGCGACTCCTGCTAACTCT-3' 5'-AGAGTTAGCAGGAGTCGCATGGCTATCTAAATTGTC-3'	Protein expression
pET28a-v2c-H408A	5'-ATGCTTCCAGAAGACGCGCGAGCTACACTCTCATAT-3' 5'-TGAGAGTGTAGCTCGCGCGTCTTCTGGAAGCAT-3'	Protein expression

Restriction enzyme sites are underlined. UF (upstream forward), UR (upstream reverse), DF (downstream forward) and DR (downstream reverse).